Geochemical Evidence for Slab Melting in the Trans-Mexican Volcanic Belt

ARTURO GÓMEZ-TUENA[1]*, CHARLES H. LANGMUIR[2], STEVEN L. GOLDSTEIN[3], SUSANNE M. STRAUB[3] AND FERNANDO ORTEGA-GUTIÉRREZ[4]

[1]CENTRO DE GEOCIENCIAS, UNIVERSIDAD NACIONAL AUTÓNOMA DE MÉXICO, QUERÉTARO 76230, MEXICO

[2]DEPARTMENT OF EARTH AND PLANETARY SCIENCES, HARVARD UNIVERSITY, CAMBRIDGE, MA 02138, USA

[3]LAMONT–DOHERTY EARTH OBSERVATORY AND DEPARTMENT OF EARTH AND ENVIRONMENTAL SCIENCES, COLUMBIA UNIVERSITY, 61 RT. 9W, PALISADES, NY 10964, USA

[4]INSTITUTO DE GEOLOGÍA, UNIVERSIDAD NACIONAL AUTÓNOMA DE MÉXICO, CIUDAD UNIVERSITARIA, MEXICO CITY 04510, MEXICO

Geochemical studies of Plio-Quaternary volcanic rocks from the Valle de Bravo–Zitácuaro volcanic field (VBZ) in central Mexico indicate that slab melting plays a key role in the petrogenesis of the Trans-Mexican Volcanic Belt. Rocks from the VBZ are typical arc-related high-Mg andesites, but two different rock suites with distinct trace element patterns and isotopic compositions erupted concurrently in the area, with a trace element character that is also distinct from that of other Mexican volcanoes. The geochemical differences between the VBZ suites cannot be explained by simple crystal fractionation and/or crustal assimilation of a common primitive magma, but can be reconciled by the participation of different proportions of melts derived from the subducted basalt and sediments interacting with the mantle wedge. Sr/Y and Sr/Pb ratios of the VBZ rocks correlate inversely with Pb and Sr isotopic compositions, indicating that the Sr and Pb budgets are strongly controlled by melt additions from the subducted slab. In contrast, an inverse correlation between Pb(Th)/Nd and $^{143}Nd/^{144}Nd$ ratios, which extend to lower isotopic values than those for Pacific mid-ocean ridge basalts, indicates the participation of an enriched mantle wedge that is similar to the source of Mexican intraplate basalts. In addition, a systematic decrease in middle and heavy rare earth concentrations and Nb/Ta ratios with increasing SiO_2 contents in the VBZ rocks is best explained if these elements are mobilized to some extent in the subduction flux, and suggests that slab partial fusion occurred under garnet amphibolite-facies conditions.

INTRODUCTION

Slab-derived fluxing plays an important role in the global geochemical cycle, and gives rise to the distinctive chemical compositions observed in arc magmas (Gill, 1981). However, the physical mechanism of element recycling at subduction zones remains controversial: is the subduction component a hydrous fluid, derived from the dehydration of the altered portions of the oceanic crust and its sedimentary cover? Or is it a water-rich silicate melt derived from the partial fusion of the subducted materials? Or, more complicated still, is it a combination of both hydrous fluids and silicate melts? Can we distinguish the chemical fingerprints of these two processes of element recycling in the geochemistry of arc magmas? And if a distinction can be drawn, then which reactions are involved, and how can we relate them to the thermal and tectonic conditions of a subduction zone? Arcs constructed over thick continental crusts provide additional complications because mantle-derived melts could stagnate, differentiate and assimilate pre-existing rocks at various depths along their journey to the surface, in a process that can obscure the chemical

*Corresponding author. Telephone: (5255) 5623-4104 ext. 120. Fax: (5255) 5623-4101. E-mail: tuena@geociencias.unam.mx

imprints of the subduction environment. Is it possible to distinguish the chemical contributions of the continental crust from those derived from the subduction flux? Answering all these questions is essential for understanding and quantifying the solid-earth geochemical cycle on a global scale, and they have implications for more complicated questions such as the origin of the continental crust.

In this contribution we provide new geochemical data from the Valle de Bravo–Zitácuaro volcanic field (VBZ), a Pliocene to Quaternary monogenetic field located in the central sector of the Trans-Mexican Volcanic Belt (TMVB). The rocks in this area have major element compositions that are typical of arc volcanic rocks worldwide, and are similar to andesitic rocks erupted from long-lived Mexican stratovolcanoes. They are thus representative of the current tectonic and geological conditions that generate andesitic magmas in the central sector of the TMVB, and are an excellent suite to address magma generation processes in a thick-crusted continental arc. We will show that crystal fractionation and/or crustal contamination did not play a significant role in their petrogenesis, but that the geochemical signatures are better explained by different proportions of slab-derived silicate melts reacting with the sub-arc mantle wedge.

TECTONIC AND GEOLOGICAL SETTING

The Mexican subduction zone is a natural laboratory to test the efficiency with which chemical elements are subducted and ultimately recycled into arc magmas because parameters that govern its thermal structure gradually change along-strike (Fig. 1). The age and convergence rate of the subducted Rivera and Cocos plates gradually increase eastward along the trench, as the dip angle decreases to a sub-horizontal plane (Pardo & Suárez, 1995). Although the Wadati–Benioff zone below central Mexico is poorly defined, it has been long considered that the current volcanic front emerges when the subducted slabs reach ∼100 km depth, despite significant differences in the subduction angle. Recent thermal models and new focal data compilations have suggested, however, that the slab depth below central Mexico could be as shallow as 70–80 km, and that slab melting could occur at those depths (Manea et al., 2004, 2005). Indeed, slab melting has recently been invoked to explain the origin of some Miocene and Quaternary rock sequences along the arc (Luhr, 2000; Gómez-Tuena et al., 2003; Martínez-Serrano et al., 2004).

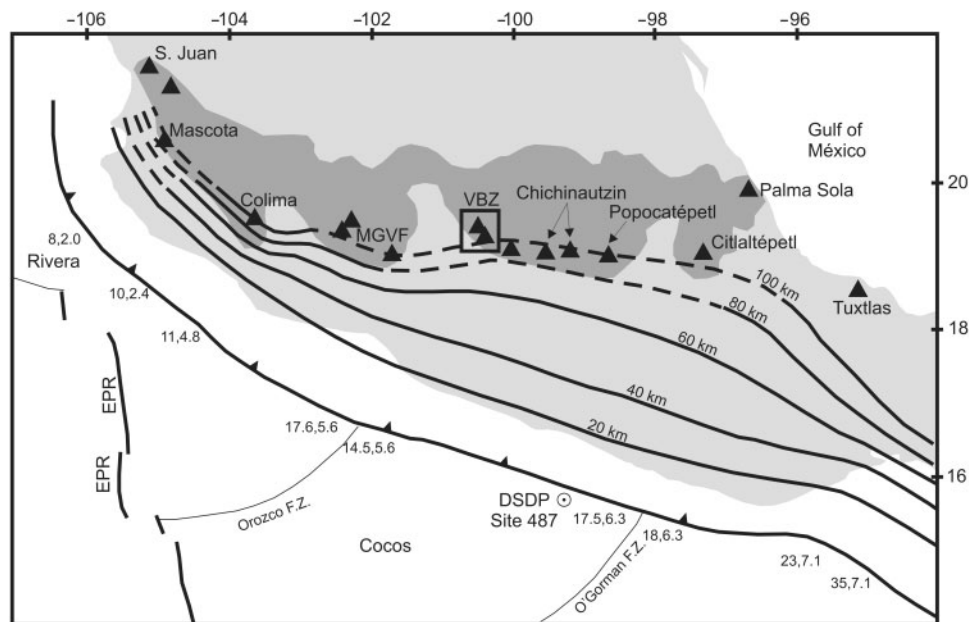The compositional variability and the mass of the sediment fill that is subducted are not well known,

Fig. 1. Generalized map of the Trans-Mexican Volcanic Belt (dark shading) and main tectonic features of the Rivera and Cocos plates [modified from Pardo & Suárez (1995)]. Numbers separated by a comma along the trench indicate the age of the oceanic crust (in Ma) and the convergence rate (in cm/year), respectively. Contours represent the depth of the top of the subducted slab (segmented when inferred). The studied area is depicted by a box labelled Valle de Bravo–Zitácuaro volcanic field (VBZ). A representative section of the subducted sediments and altered oceanic crust was sampled by the Deep Sea Drilling Project at Site 487 (DSDP Site 487). Also shown are the locations of some important volcanic fields: Palma Sola volcanic field (Palma Sola), Los Tuxtlas volcanic field (Tuxtlas), Citlaltépetl volcano (Citlaltépetl), Popocatépetl volcano (Popocatépetl), Chichinautzin volcanic field (Chichinautzin), Michoacán–Guanajuato volcanic field (MGVF), Colima volcano (Colima), Mascota volcanic field (Mascota), and San Juan volcano (S. Juan).

but evidence from gravimetric profiles indicates that the sediment column could be as thin as ∼17 m above the young Rivera plate, and that the sediment thickness gradually increases eastwards along the trench (Manea *et al.*, 2003). In addition, Leg 66 of the Deep Sea Drilling Project (DSDP) retrieved six cores off the coast of Acapulco (Moore *et al.*, 1982). DSDP Site 487 (location shown in Fig. 1) reached into the basaltic basement. The sedimentary column of Site 487 has been described and geochemically analyzed (Moore & Shipley, 1988; Plank & Langmuir, 1998; Verma, 2000*b*; LaGatta, 2003), and consists of two units: ∼100 m of continentally derived Quaternary hemipelagic sediments that rest above ∼70 m of late Miocene–Pliocene pelagic sediments. Fragments of altered oceanic crust (AOC) from Site 487 have been described and analyzed, and are mainly composed of an olivine- and plagioclase-bearing basalt with minor amounts of an aphyric basalt (Verma, 2000*b*; LaGatta, 2003).

The VBZ is currently one of the best studied areas of the TMVB. Recent publications have mapped and addressed the local geology, stratigraphy, petrography, and the major and trace element geochemistry of the volcanic successions (Capra *et al.*, 1997; Blatter & Carmichael, 1998*b*; Blatter *et al.*, 2001). Furthermore, primitive andesites from the VBZ have also been studied experimentally (Blatter & Carmichael, 2001). In summary, the volcanism in the area is characterized by a myriad of cinder cones, domes and isolated fissural lava flows of andesite–dacite compositions with ages that vary between 5 ka and 6 Ma. The experimentally determined hydrous phase equilibria of the VBZ andesites are suggestive of pre-eruptive H_2O contents of 2·5–6 wt %, and the varied phenocryst assemblages in the lavas appear to be the result of water loss during decompression and ascent (Blatter & Carmichael, 2001). The excellent match between the amount of crystals in the natural rocks and the experiments strongly suggests that the lavas are true liquid compositions. Importantly, Blatter & Carmichael (2001) suggested a direct mantle origin for some of the VBZ andesites on the basis of the high Ni and Cr abundances of the volcanic rocks, the presence of nodules of amphibole-bearing peridotite in one of the andesitic lava flows (Blatter & Carmichael, 1998*a*), and the similarity of compositions between the VBZ lavas and experimental water-saturated lherzolite melts (Hirose, 1997).

SAMPLES AND ANALYTICAL METHODS

In this contribution we report comprehensive geochemical data for the youngest volcanic sequences of the Valle de Bravo Zitácuaro volcanic field (<3·77 Ma),

as geologically characterized by Capra *et al.* (1997) and Blatter *et al.* (2001). We deliberately exclude the older and more altered volcanic successions (6–3·77 Ma).

Major element compositions for most samples were obtained by X-ray fluorescence (XRF) using a Siemens SRS-3000 instrument at Instituto de Geología, UNAM, following procedures described elsewhere (Lozano *et al.*, 1995). Trace element abundances were determined by inductively coupled plasma mass spectrometry (ICP-MS) using a VG-PQ2+ at the Lamont–Doherty Earth Observatory (LDEO), following sample preparation and measurement procedures described by Gómez-Tuena *et al.* (2003). Additional major and trace element data were obtained by ICP-MS at Activation Laboratories of Ancaster, Canada (http://www.actlabs.com/) employing lithium metaborate/tetraborate fusions. Boron concentrations on selected samples were obtained by prompt gamma neutron activation (PGNA) at Activation Laboratories. Reproducibility is better than 10% for Li, Be, Sc, Cr, Ni, Cu, Zn, Mo, Sb, Cs, Tl and Pb, and better than 3% for all other elements. Typical precision for B is 100% at 0·5 ppm, 15% at 5 ppm, and better than 5% at 50 ppm.

Sr, Nd and Pb isotopic compositions were determined by thermal ionization mass spectrometry (TIMS) at LDEO using a VG sector 54-30 system equipped with nine Faraday collectors, following sample preparation and measurement procedures described by Gómez-Tuena *et al.* (2003). $^{87}Sr/^{86}Sr$ ratios are normalized to $^{86}Sr/^{88}Sr = 0·1194$ and adjusted to an NBS987 standard ratio of 0·710230. During two separated intervals of analyses, the measured values of the NBS987 standard were $^{87}Sr/^{86}Sr = 0·710245 \pm 0·000016$ (2σ, $n = 4$) and 0·710271 $\pm$ 0·000014 (2σ, $n = 6$). $^{143}Nd/^{144}Nd$ ratios were normalized to $^{146}Nd/^{144}Nd = 0·72190$ and corrected to a La Jolla Standard value of $^{143}Nd/^{144}Nd = 0·511860$. Over the course of this study, the measured $^{143}Nd/^{144}Nd$ ratio of La Jolla standard was 0·511836 $\pm$ 0·000013 (2σ, $n = 15$). Pb isotopic ratios were corrected for mass fractionation using the LDEO $^{207}Pb–^{204}Pb$ double spike. Using this technique, samples are analyzed twice: once mixed with the double spike and once without it. The fractionation corrected values were adjusted to NBS981 standard values of $^{206}Pb/^{204}Pb = 16·9356$, $^{207}Pb/^{204}Pb = 15·4891$, and $^{208}Pb/^{204}Pb = 36·7006$ (Todt *et al.*, 1996). Over the course of this study, the double-spike fractionation corrected Pb isotope ratios of the NBS-981 standard were $^{206}Pb/^{204}Pb = 16·9356 \pm 0·0048$ (143 ppm), $^{207}Pb/^{204}Pb = 15·4912 \pm 0·0047$ (152 ppm), and $^{208}Pb/^{204}Pb = 36·7025 \pm 0·014$ (191 ppm) (2σ, $n = 13$). Total procedural blanks between 300 and 500 pg for Pb were negligible compared with the concentrations of this element in the dissolved rock samples.

RESULTS

Detailed petrographic descriptions of the VBZ rock suite have been reported in several previous publications (Capra *et al.*, 1997; Blatter & Carmichael, 1998*a*, 1998*b*; Blatter & Carmichael, 2001; Blatter *et al.*, 2001), and the main phenocryst assemblage and modal proportions of the rocks analyzed in this study are given in Table 1. Major and trace element abundances and Sr–Nd–Pb isotopic compositions are reported in Tables 2 and 3. Overall, the VBZ rocks vary from highly porphyritic to nearly aphyric, with the least evolved andesites having a phenocryst mineralogy of olivine (Ol) and orthopyroxene (Opx), or clinopyroxene (Cpx) and Opx. More evolved andesites and dacites usually contain Opx, Cpx, occasional hornblende (Hbl) and rare biotite (Bi). Importantly, most of the lavas do not contain plagioclase as a phenocryst, a remarkable feature that was previously noted by Blatter & Carmichael (1998*b*). Nevertheless, plagioclase is commonly observed in the groundmass, forming a trachytic texture along with glass and opaque minerals. All kinds

Table 1: Modal mineralogy of the Valle de Bravo–Zitácuaro volcanic rocks

Sample	Ol	Pl	Cpx	Opx	Hbl	Bi	Op	Qtz-xen	Gms
VBZ-LRE									
Zit-99-1A	–	0·1	1·7	4	–	–		–	94·0
Zit-99-2	–	1	1	1·7	–	–		–	96·2
Zit-99-3	0·2	–	0·7	1·5	–	–		1·5	95·9
Zit-99-5	–	–	–		0·1	–		–	99·9
Zit-99-17	–	11·5	2·8	2·4	–	–		–	83·2
Zit-99-18	–	4·2	–		2	1		0·1	92·5
Zit-99-20	–	–	0·5	0·9	–	–		–	98·3
Zit-99-23	–	0·2	0·4	0·7	0·6	–	0·7	0·2	96·9
Zit-99-28	–	0·1	0·2	1·3	–	–		0·2	98·1
Zit-99-31	2·5	0·1	–		–	–		6·4	90·8
Zit-99-30	0·1	–	0·7	1·5	–	–		–	97·5
VBZ-HRE									
Zit-99-25	–	0·5	1	1·6	–	–		–	96·7
Zit-99-8	3·9	–	1·5	0·5	–	–		–	94·0
Zit-99-9	0·1	–	–	1·7	–	–		0·7	97·5
Zit-99-10	–	–	0·1	3·5	2·2	–	0·3	–	93·6
Zit-99-12	–	–	0·5	1·5	–	–		–	98·0
Zit-99-14	5·9	–	–	0·2	–	–		0·5	93·3
Zit-99-25	–	0·5	1	1·6	–	–		–	96·7
Zit-99-26	4	–	–	0·4	–	–	–	1·5	94·0

Modal proportions of phenocrysts (>0·3 mm) from a minimum of 1200 points. Ol, olivine; Pl, plagioclase; Cpx, clinopyroxene; Opx, orthopyroxene; Hbl, hornblende; Bi, biotite; Qtz-xen, quartz xenocrysts; Op, opaque minerals; Gms, groundmass.

of rocks often have small but ubiquitous quartz xenocrysts; some quartzites and schists, which were apparently entrained from the locally exposed basement, are also included as xenoliths. These nodules are often surrounded by a pyroxene shield and/or a glassy aureole, but sharp edges along the contact with the host magma are also commonly observed. These features indicate that the xenoliths were rapidly incorporated into the ascending and cooling magma shortly before eruption.

Like many arcs around the world, the igneous rocks from the VBZ belong to the subalkaline magmatic series (Fig. 2a) and do not display FeO-total enrichment during differentiation, plotting within the calc-alkaline field in an AFM diagram (not shown). The major element compositions of the VBZ rocks are very similar to those observed in the large Mexican stratovolcanoes, classified mostly as andesites and dacites, but some of the least evolved rocks from the VBZ tend to have higher K_2O contents at relatively low SiO_2 contents (Fig. 2b). These latter lavas were classified as shoshonites by Blatter *et al.* (2001).

VBZ trace elements show relative enrichments of the large ion lithophile elements (LILE) over the high field strength elements (HFSE) that are typical of arc lavas (Fig. 3); nonetheless, a close examination of the trace element systematics allows the recognition of two chemically different rock suites, herein named as VBZ high rare earth element (REE) series (VBZ-HRE) and VBZ low REE series (VBZ-LRE). The VBZ-HRE rocks tend to have higher Sr, Ba and REE contents and show distinctively strong Zr–Hf negative anomalies, an unusual feature that has not been previously observed in other TMVB rock suites (Figs 2f and 3b). VBZ-LRE andesites tend to have high Sr/Y ratios at low Y contents (Fig. 4a), a feature often observed in volcanic arcs where young and hot slabs are being subducted, and where a slab-melt component has been interpreted as the subduction agent (Defant & Drummond, 1990; Martin, 1999). VBZ-HRE rocks share the high Sr/Y ratios but they also extend to higher Y contents. Although the VBZ rocks display light and middle rare earth element (LREE–MREE) enrichments over the heavy rare earth elements (HREE) (Fig. 4b), this fractionation is not as strong as observed in 'adakite-like' magmas of the Miocene TMVB (Gómez-Tuena *et al.*, 2003) or the Andean Austral Volcanic Zone (Stern & Kilian, 1996); but it is comparable with that in high-Mg andesites from Adak island in the Aleutians (Kay, 1978) and from Mount St. Helens in the Cascades (Smith & Leeman, 1996).

Relationships between Sr, Nd, and Pb isotope ratios and possible end-member components are shown in Fig. 5. Overall, the Sr–Nd isotopic ratios of the VBZ are bracketed between the compositions of East Pacific Rise mid-ocean ridge basalts (EPR-MORB) and an enriched 'crustal component', similar in composition to Mexican

Table 2: *Major and trace element compositions of the Valle de Bravo–Zitácuaro volcanic rocks*

Sample:	ZIT-99-1a	ZIT-99-1B*	ZIT-99-2	ZIT-99-3	ZIT-99-5	ZIT-99-17*	ZIT-99-18	ZIT-99-19*	ZIT-99-20*	ZIT-99-23*
Unit:	VBZ-LRE	VBZ-LRE	VBZ-LRE	VBZ-LRE	VBZ-LRE	VBZ-LRE	VBZ-LRE	VBZ-LRE	VBZ-LRE	VBZ-LRE
Long. W:	100·20	100·20	100·22	100·26	100·28	100·15	100·16	100·20	100·34	100·39
Lat. N:	19·22	19·22	19·19	19·18	19·10	19·40	19·40	19·45	19·43	19·32
Locality:	C. El Rosario	C. El Rosario	Colorines	Sto. Tomás Plátanos	Agua Zarca	Sta. María Delicias	Arroyo Lindero	La Dieta	Pueblo Nuevo	El Álamo
SiO_2	62·1	63·9	62·0	64·7	62·6	61·2	63·2	60·5	62·2	64·2
TiO_2	0·7	0·6	0·6	0·6	0·7	0·7	0·6	0·6	0·6	0·5
Al_2O_3	16·1	15·9	16·1	16·0	17·7	16·6	16·9	18·4	16·3	16·4
Fe_2O_{3T}	5·4	4·4	5·3	4·2	4·8	5·5	4·2	4·5	4·6	4·0
MnO	0·08	0·07	0·08	0·06	0·07	0·08	0·07	0·07	0·07	0·07
MgO	4·9	3·6	5·1	3·4	2·5	3·0	2·8	2·0	3·9	3·1
CaO	5·9	5·1	5·8	5·4	5·3	5·6	5·1	4·5	5·5	4·6
Na_2O	3·7	4·2	3·7	3·9	4·2	3·5	4·0	3·5	3·8	4·3
K_2O	1·5	1·8	1·8	1·8	2·2	1·9	1·7	1·6	2·1	2·3
P_2O_5	0·1	0·2	0·1	0·1	0·2	0·1	0·1	0·1	0·1	0·2
LOI	0·3	0·3	0·0	0·0	0·0	1·5	0·9	4·7	0·9	0·0
Total	100·7	100·0	100·6	100·0	100·3	99·7	99·5	100·6	100·2	99·5
Sc		12								
V	104	78	115	85	104	82	74	52	82	51
Cr		100				62			92	66
Co	19·7	13·7	19·0	14·0	11·7	11·2	12·0	6·5	13·6	9·6
Ni	120	55	50	61		24	34		49	54
Cu	20	19	22	36	12	16	18		27	16
Zn	88	53	64	66	59	52	43	47	53	48
Ga	18·4	17·7	19·1	18·6	21·4	15·9	20·0	15·8	17·2	16·6
Li	9·0		8·6	8·0	14·1		16·6			
Be	1·1	1·0	1·4	1·1	1·5	1·3	1·5			
B	10·6	8·1	3·0	5·9	6·8	3·8	9·9			9·0
Rb	21·3	26·6	28·8	21·8	32·5	44·6	28·4	28·1	27·3	30·4
Sr	797	683	778	878	799	471	828	457	754	699
Y	14·8	12·6	15·7	10·8	13·6	15·7	12·6	11·5	10·5	10·0
Zr	103	125	127	106	149	126	108	105	107	121
Nb	4·33	3·52	4·01	2·90	4·35	4·24	4·31	3·41	2·88	3·13
Mo	0·81		0·60	0·56	0·83		0·49			
Sn	0·33		0·94	0·63	0·86	1·33	0·71			
Sb	0·02		0·06	0·05	0·10		0·07			1·99
Cs	0·43	0·64	0·93	0·44	1·26	0·90	2·18	1·93	1·06	1·19
Ba	364	382	391	367	453	361	489	601	420	473
La	13·17	12·86	13·18	10·46	14·73	12·48	14·64	11·24	11·68	14·65
Ce	28·30	26·43	28·31	22·13	31·57	25·31	30·11	20·55	23·99	29·43
Pr	3·64	3·44	3·66	2·91	4·05	3·61	3·87	3·07	3·32	3·71
Nd	15·03	13·36	15·08	12·12	16·66	14·39	15·53	11·83	13·17	13·78
Sm	3·19	2·78	3·24	2·62	3·56	3·20	3·17	2·50	2·69	2·52
Eu	1·02	0·97	1·01	0·88	1·13	0·93	1·03	0·88	0·91	0·85
Gd	3·01	2·66	3·02	2·37	3·12	3·09	2·76	2·38	2·46	2·24
Tb	0·46	0·40	0·47	0·35	0·45	0·48	0·41	0·36	0·36	0·32
Dy	2·60	2·24	2·71	2·00	2·42	2·73	2·21	2·02	1·96	1·76
Ho	0·51	0·43	0·54	0·38	0·48	0·52	0·43	0·39	0·36	0·33
Er	1·42	1·31	1·49	1·05	1·30	1·55	1·16	1·17	1·07	1·02
Tm		0·19				0·24		0·17	0·15	0·15
Yb	1·33	1·20	1·50	1·06	1·25	1·44	1·17	1·10	1·00	1·00
Lu	0·208	0·180	0·230	0·162	0·190	0·206	0·179	0·158	0·142	0·140
Hf	2·93	3·25	3·52	3·01	3·98	3·28	3·15	2·86	2·87	3·12
Ta	0·273	0·233	0·282	0·210	0·291	0·340	0·337	0·283	0·198	0·222
W	0·143		0·226	0·109	0·179		0·124			
Tl	0·056	0·079	0·207	0·134	0·194	0·218	0·209	0·284	0·171	0·238
Pb	4·00		10·54	5·79	7·44	5·29	7·24	7·91	6·31	7·51
Th	2·19	3·02	3·33	1·97	3·58	3·67	2·93	2·85	2·40	3·32
U	0·476	0·831	0·980	0·682	0·971	1·123	1·017	1·117	0·793	0·982

(continued)

Sample:	ZIT-99-28*	ZIT-99-29*	ZIT-99-27*	ZIT-99-31	ZIT-99-30	ZIT-99-25	ZIT-99-7*	ZIT-99-8	ZIT-99-9	ZIT-99-10
Unit:	VBZ-LRE	VBZ-LRE	VBZ-LRE	VBZ-LRE	VBZ-LRE	VBZ-HRE	VBZ-HRE	VBZ-HRE	VBZ-HRE	VBZ-HRE
Long. W:	100·43	100·47	100·44	100·49	100·49	100·47	100·07	100·06	100·09	100·10
Lat. N:	19·39	19·49	19·41	19·41	19·42	19·44	19·07	19·05	19·03	19·04
Locality:	C. Los Coyotes	La Garita	El Asoleadero	C. El Molcajete	La Soledad	Las Pilas	Sn. Fr. La Albarrada	Temascaltepec	C. Tezontle	El Peñón
SiO$_2$	60·5	54·6	60·8	54·2	59·8	58·0	51·6	54·2	58·8	59·3
TiO$_2$	0·7	1·3	0·8	1·1	0·8	0·9	0·8	0·9	0·9	0·9
Al$_2$O$_3$	16·3	16·9	16·0	17·0	16·3	15·1	16·3	15·9	17·2	16·1
Fe$_2$O$_{3T}$	5·3	8·4	5·2	8·0	5·7	5·6	7·6	7·4	6·2	6·4
MnO	0·09	0·12	0·09	0·13	0·09	0·08	0·13	0·11	0·09	0·10
MgO	4·1	5·8	4·2	6·7	4·9	6·2	8·7	7·5	4·4	4·2
CaO	6·1	7·4	6·3	7·1	5·6	7·8	8·8	7·8	6·1	6·8
Na$_2$O	3·3	3·6	3·6	3·5	4·0	3·5	3·2	3·6	3·9	3·6
K$_2$O	2·3	1·4	2·0	1·4	1·7	1·8	2·0	2·4	2·1	1·8
P$_2$O$_5$	0·1	0·3	0·2	0·2	0·2	0·3	0·4	0·4	0·3	0·3
LOI	0·8	−0·1	0·9	0·4	0·6	0·6	0·3	0·4	0·7	0·7
Total	99·8	99·8	100·0	99·6	99·7	99·9	99·9	100·5	100·8	100·2
Sc			17				24			
V	128	133	131	144	86	118	184	159	114	144
Cr		129	106				381			
Co	16·3	26·1	16·3	28·3	19·9	24·3	32·2	31·5	18·4	20·9
Ni	45	80	67	153	140	155	167	201	88	66
Cu	23	31	25	34	30	42	46	48	31	47
Zn	47	83	60	70	87	47	74	84	64	89
Ga	18·9	17·7	18·0	18·4	18·9	20·1	15·7	18·9	20·3	20·7
Li	7·1			10·4	10·2	9·5		13·0	13·4	9·0
Be	1·2	1·3	1·0	1·3	1·5	1·6	1·0	1·9	2·2	1·8
B	7·0	7·7	5·2		9·8	5·5	3·8	3·8	12·2	7·1
Rb	23·5	21·7	22·9	21·0	30·7	24·6	35·3	37·6	31·3	25·5
Sr	890	576	863	653	655	1847	818	1088	1002	1244
Y	15·8	22·2	15·1	23·2	15·1	16·7	18·6	23·1	29·9	28·9
Zr	106	164	110	144	138	153	133	171	188	162
Nb	3·04	7·35	3·19	10·87	4·89	4·21	3·14	5·90	7·08	4·67
Mo	0·56			1·19	0·61	0·75		0·92	1·07	0·64
Sn	0·62	1·20		0·90	0·94	0·95		1·04	1·15	1·15
Sb	0·04			0·03	0·06	0·04	0·28	0·04	0·12	0·06
Cs	0·91	0·57	0·79	0·60	0·87	0·70	1·38	0·80	1·16	0·89
Ba	379	381	398	342	472	556	654	895	729	469
La	11·87	16·27	11·58	14·91	14·17	33·15	30·86	44·87	55·14	35·32
Ce	25·51	34·24	24·99	32·39	29·91	73·94	62·33	91·89	102·98	58·78
Pr	3·58	4·71	3·45	4·27	4·01	9·86	8·37	12·04	14·28	9·49
Nd	15·22	18·88	14·16	18·00	16·94	40·49	32·35	48·76	56·72	39·44
Sm	3·38	4·18	3·08	4·06	3·58	7·03	6·04	8·92	10·17	7·14
Eu	1·11	1·38	1·10	1·36	1·18	2·01	1·80	2·46	2·88	2·07
Gd	3·11	4·10	2·95	4·01	3·24	5·18	4·99	6·82	8·16	6·34
Tb	0·47	0·67	0·47	0·64	0·48	0·69	0·66	0·90	1·14	0·89
Dy	2·85	3·82	2·72	3·85	2·70	3·14	3·45	4·24	5·63	4·91
Ho	0·54	0·72	0·53	0·78	0·51	0·57	0·64	0·77	1·03	0·95
Er	1·54	2·17	1·56	2·23	1·41	1·42	1·85	2·01	2·68	2·58
Tm		0·32	0·24				0·26			
Yb	1·55	1·94	1·48	2·17	1·37	1·38	1·69	1·80	2·50	2·48
Lu	0·242	0·285	0·222	0·338	0·203	0·202	0·242	0·271	0·375	0·366
Hf	3·04	3·70	2·89	3·40	3·59	4·21	3·33	4·23	4·62	4·54
Ta	0·206	0·512	0·169	0·626	0·332	0·255	0·183	0·326	0·421	0·316
W	0·097			0·185	0·155	0·108		0·207	0·582	0·247
Tl	0·131	0·133	0·128	0·109	0·237	0·141	0·164	0·225	0·216	0·088
Pb	6·03	5·88	5·49	4·65	7·41	7·84	7·96	11·53	9·13	5·87
Th	2·21	2·43	2·22	2·04	2·13	3·87	6·00	6·00	4·78	3·03
U	0·772	0·724	0·751	0·592	0·867	1·140	1·838	1·942	1·542	1·015

(continued)

Sample:	ZIT-99-11*	ZIT-99-12	ZIT-99-14	ZIT-99-24*	ZIT-99-26
Unit:	VBZ-HRE	VBZ-HRE	VBZ-HRE	VBZ-HRE	VBZ-HRE
Long. W:	100·14	100·19	100·25	100·45	100·46
Lat. N:	19·03	19·05	19·07	19·46	19·43
Locality:	C. Pelón	Potrero de Tenayac	C. Pelón	Agua Salada	Las Pilas
SiO_2	52·6	56·4	54·9	55·1	55·7
TiO_2	1·0	0·9	0·8	1·3	1·1
Al_2O_3	15·0	16·4	15·4	16·9	15·5
Fe_2O_{3T}	7·4	6·6	7·4	7·9	7·0
MnO	0·12	0·09	0·11	0·12	0·10
MgO	8·9	5·1	8·9	4·8	5·6
CaO	9·0	6·7	7·4	7·3	6·8
Na_2O	3·6	3·9	3·2	3·7	3·6
K_2O	1·5	2·5	1·3	1·4	2·8
P_2O_5	0·4	0·4	0·2	0·4	0·4
LOI	0·2	0·7	0·4	0·6	0·9
Total	99·5	99·6	100·2	99·4	99·6
Sc	22			19	
V	153	135	150	150	151
Cr	438			106	
Co	33·6	22·2	33·6	23·2	32·2
Ni	184	90	223	48	182
Cu	43	43	47	28	34
Zn	73	91	72	94	80
Ga	16·6	21·0	17·2	19·6	20·5
Li		11·8	6·2		9·7
Be	1·1	2·7	1·3	1·2	2·8
B	1·9	9·2	9·0	5·5	7·9
Rb	20·3	37·8	21·2	25·4	52·8
Sr	1230	1032	770	631	1301
Y	19·2	38·9	19·8	23·7	32·9
Zr	121	177	137	199	246
Nb	4·12	6·06	4·81	9·32	4·92
Mo		0·98	0·76		0·79
Sn	1·25	1·12	0·77	1·44	1·38
Sb		0·18	0·10		0·05
Cs	0·53	1·47	1·11	0·67	0·96
Ba	590	887	434	425	993
La	30·26	79·51	24·47	20·84	46·85
Ce	63·25	155·45	47·88	43·75	95·78
Pr	8·64	19·78	6·69	5·97	12·64
Nd	33·09	79·58	26·88	23·75	51·90
Sm	6·17	14·71	5·16	5·08	9·80
Eu	1·82	3·82	1·56	1·62	2·79
Gd	4·98	12·10	4·48	4·82	8·16
Tb	0·66	1·61	0·64	0·74	1·13
Dy	3·53	8·24	3·40	4·25	5·89
Ho	0·63	1·44	0·67	0·80	1·06
Er	1·84	3·64	1·78	2·43	2·75
Tm	0·25			0·36	
Yb	1·61	3·26	1·69	2·20	2·54
Lu	0·233	0·459	0·260	0·319	0·361
Hf	3·09	4·80	3·38	4·42	6·61
Ta	0·245	0·377	0·285	0·644	0·353
W		0·193	0·197		0·169
Tl		0·271	0·238	0·201	0·280
Pb	5·89	10·57	5·76	6·73	8·57
Th	3·56	5·50	2·99	2·58	4·07
U	1·059	1·779	0·943	0·783	1·704

Major elements (in wt %) were analyzed by XRF. Trace elements (in ppm) were analyzed by ICP-MS.
*Samples analyzed by ICP-MS for major and trace elements at Activation Laboratories, Canada. Boron analyzed by prompt gamma neutron activation (PGNA) at Activation Laboratories, Canada.

Table 3: Sr, Nd and Pb isotope compositions of the Valle de Bravo–Zitácuaro volcanic rocks

	$^{87}Sr/^{86}Sr$	2σ	$^{206}Pb/^{204}Pb$	$^{207}Pb/^{204}Pb$	$^{208}Pb/^{204}Pb$	$^{143}Nd/^{144}Nd$	2σ
VBZ-LRE							
ZIT-99-1a	0·703377	12	18·5921	15·5654	38·2915		
ZIT-99-2	0·703469	10	18·6342	15·5775	38·3526	0·512832	16
ZIT-99-3	0·703223	10	18·5605	15·5547	38·2151	0·512891	16
ZIT-99-5	0·703523	10	18·5847	15·5609	38·2773	0·512833	20
ZIT-99-28	0·703397	12	18·5598	15·5597	38·2240	0·512914	10
ZIT-99-31	0·703663	10	18·6462	15·5776	38·3761	0·512853	12
ZIT-99-30	0·704321	12	18·6372	15·5822	38·3509	0·512794	16
VBZ-HRE							
ZIT-99-25	0·703306	10	18·5713	15·5584	38·2462	0·512978	8
ZIT-99-8	0·704355	10	18·6755	15·5879	38·4227	0·512893	18
ZIT-99-9	0·703847	10	18·6489	15·5787	38·3629	0·512891	12
ZIT-99-10	0·703351	12	18·6019	15·5627	38·2872	0·512930	14
ZIT-99-12	0·704253	10	18·6554	15·5782	38·3770	0·512876	14
ZIT-99-14	0·703692	12	18·6362	15·5710	38·3424	0·512899	18
ZIT-99-26	0·704217	10	18·6324	15·5759	38·3326	0·512876	12

2σ errors for individual Sr and Nd measurements are multiplied by 10^6. Reproducibility for Pb isotopes are given by the double-spike fractionation corrected composition of the NBS981 standard $^{206}Pb/^{204}Pb = 16·9356 \pm 0·0048$ (143 ppm), $^{207}Pb/^{204}Pb = 15·4912 \pm 0·0047$ (152 ppm), $^{208}Pb/^{204}Pb = 36·7025 \pm 0·014$ (191 ppm) (2σ, $n = 13$). Pb values were adjusted to NBS981 standard values of Todt *et al.* (1996).

lower crustal xenoliths and high-grade metamorphic terranes, or to the bulk subducted sediment sampled at DSDP Site 487. Pb isotopes form a tight positive correlation bracketed by EPR-MORB and our estimate of the average value for Site 487 sediments (which could also represent a crustal component) (Fig. 5c and d). Sr and Pb isotopic compositions largely overlap within the suites, but the Nd isotope compositions of the VBZ-HRE rocks appear to be slightly shifted towards higher values at a given $^{87}Sr/^{86}Sr$ ratio. Interestingly, rocks from the VBZ tend to overlap the compositions observed at Popocatépetl stratovolcano but they also extend to relatively lower Sr and Pb isotope ratios at similar $^{143}Nd/^{144}Nd$ ratios.

DISCUSSION

The overall trace element patterns of VBZ lavas are typical of arc-related andesites, for example with Nb–Ta depletions, Pb enrichments, and high Sr/Nd and Ba/LREE (Fig. 3). However, different VBZ rock suites with distinct trace element patterns and isotopic compositions erupted concurrently in the area. In addition, VBZ lavas display compositions that are different from other Mexican stratovolcanoes (Fig. 4). For example, VBZ lavas tend to have higher Sr/Y and Sm/Y ratios, but lower Cs/La and Rb/Ba ratios than Popocatépetl lavas at similar

fractionation levels. The geochemical differences observed within the VBZ rocks, and at different geographical positions within the arc, might be related to variations in the subduction geochemical fluxes, or they might be governed by different components and processes that operate during magma ascent through the upper plate (i.e. crystal fractionation, crustal melting and/or contamination). In this section we discuss the different components and processes that controlled the compositions of the VBZ rocks and provide a quantitative model for their petrogenesis.

Crystal fractionation and crustal contamination

Several workers have recognized that a significant part of the geochemical variability observed in continental arcs could be attributed to a process of crustal melting and/or assimilation, such that the chemical imprints derived from the subduction environment are largely obscured (Hildreth & Moorbath, 1988). Indeed, based on isotopic and trace element modeling, some workers have suggested that crustal contamination has played an important role in the petrogenesis of differentiated magmas emplaced across the TMVB (Verma, 1999, 2000*a*; Lassiter & Luhr, 2001; Chesley *et al.*, 2002; Schaaf *et al.*, 2005). Therefore, evaluating the role of magma differentiation and crustal contamination in the genesis of the studied
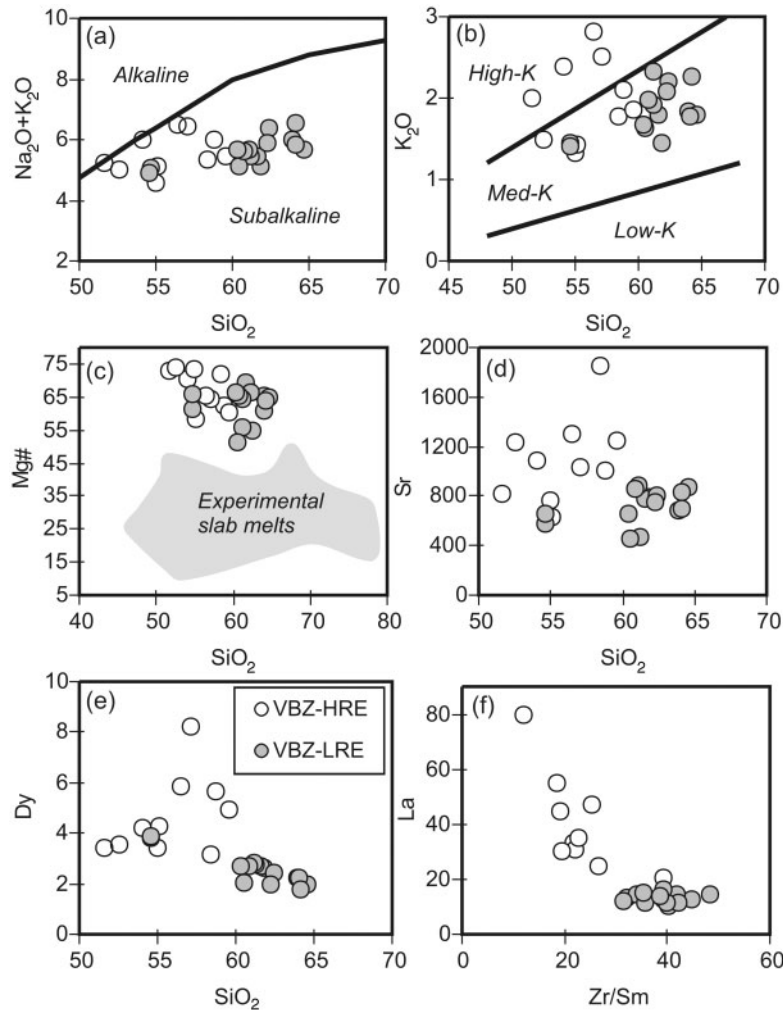
Fig. 2. Selected major element (a–c) and trace element (d–f) variation diagrams of the studied rock suites. Alkaline and subalkaline division from Irvine & Baragar (1971); K_2O vs SiO_2 classification fields from Le Maitre (1989). Grey shaded field in (c) indicates experimental melts of natural hydrous basalt at 1–4 GPa (Sen & Dunn, 1994; Rapp, 1995; Rapp & Watson, 1995; Rapp *et al.*, 1999). Calculated molar Mg-number $= Mg/(Mg + 0.85Fe^{2+}_{tot})$.

rocks is important if we aim to recognize and quantify the processes that take place at deeper levels in the subduction zone.

The geochemical trends observed in the major and trace element variation diagrams (Figs 2 and 4), together with the variability in the isotopic compositions of the two VBZ rock suites (Fig. 5), rule out simple crystal fractionation from a common primitive magma as the dominant petrogenetic process. For instance, whereas the major element compositions of both rock suites display coherent trends, Sr and REE contents are significantly higher in the VBZ-HRE than in the VBZ-LRE (Fig. 2). Clearly, these compositional differences cannot be simply accounted for by crystal fractionation from a cogenetic primitive magma, but should instead be a reflection of distinct magma source regions for both rock suites.

Atherton & Petford (1993) showed that some rocks that display slab-melt geochemical features, such as high LREE/HREE and Sr/Y ratios, could be the result of partial fusion of newly underplated, garnet-bearing, basaltic crust. Indeed, several workers have recognized that melting of a thickened crust by underplating of mantle-derived magmas can form SiO_2-rich liquids with trace element characteristics that are indistinguishable from those related to partial fusion of the subducted oceanic crust (Conrey *et al.*, 2001; Hou *et al.*, 2004; Wang *et al.*, 2005). The VBZ rocks, however, display significantly higher MgO contents (to ~9 wt %) and Mg-number (~75 to 50) that are unlike those attributed to direct partial melting of a mafic garnet-bearing lower continental crust (Mg-number <50, Fig. 2c). In addition, high Sr/Y ratios are coupled with less radiogenic Pb and
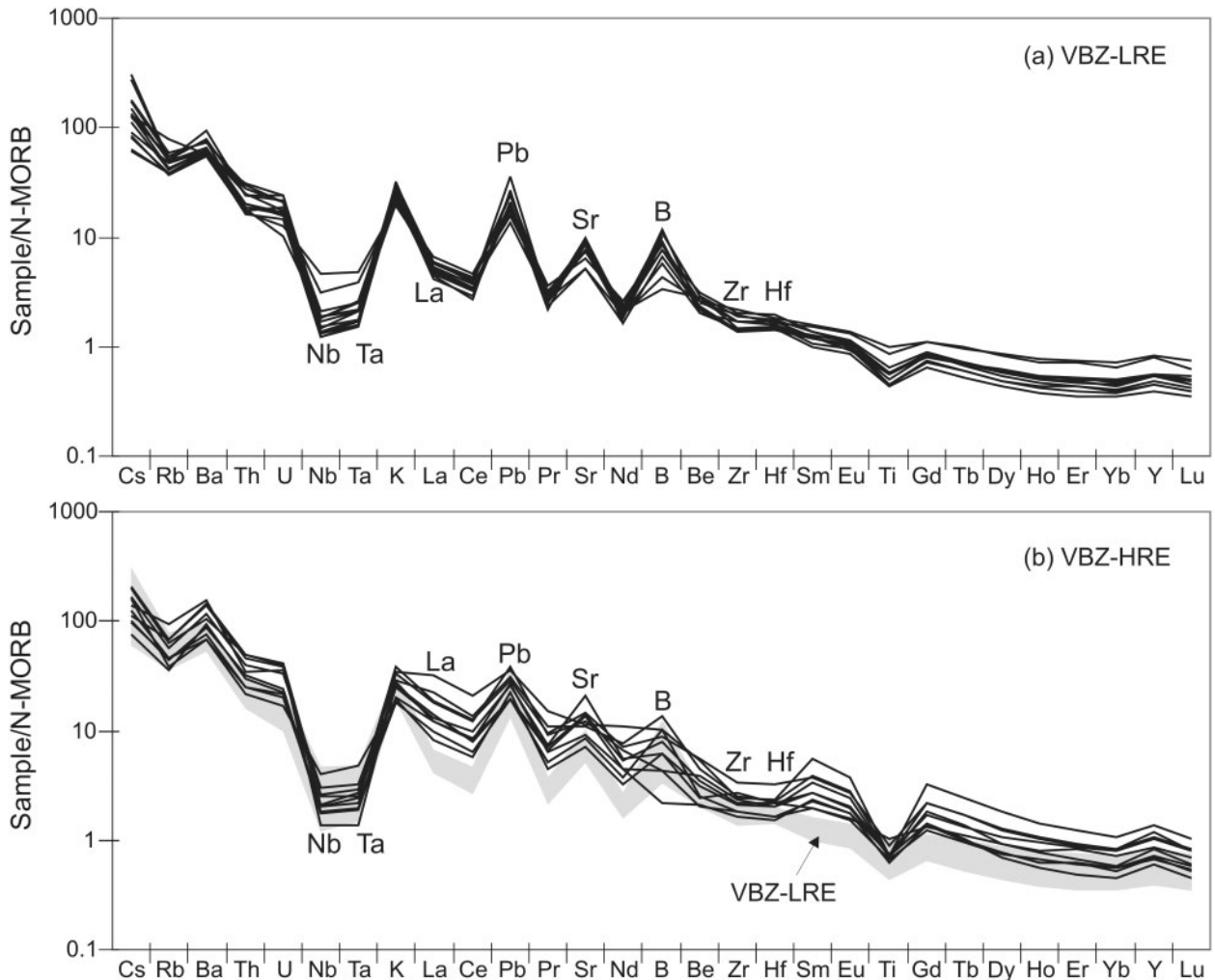
Fig. 3. N-MORB-normalized trace element patterns of the studied rock suites. (a) Valle de Bravo–Zitácuaro low REE series (VBZ-LRE); (b) Valle de Bravo–Zitácuaro high REE series (VBZ-HRE). VBZ-LRE variation field shown in grey. N-MORB values from Sun & McDonough (1989).

Sr isotopic compositions (Fig. 6), and thus the isotope ratios of the higher Sr/Y lavas trend towards the composition of Pacific MORB, and away from the isotopic compositions of lower crustal xenoliths and Mexican basement terranes (Fig. 5). Therefore, if the VBZ rocks with high Sr/Y ratios were derived from melting or assimilation of the pre-existent continental crust, the isotopic composition of the contaminant must be more like Pacific MORB than currently known Mexican basement.

Correlations between isotopic compositions and indices of fractionation are often regarded as the best indicators of crustal contamination (assimilation–fractional crystallization; AFC) because this process involves the incorporation of a magma derived from the partial fusion of the crust, and the concurrent fractionation of crystalline phases (DePaolo, 1981). However, the isotopic compositions of the VBZ are largely uncorrelated with Mg-number

(Fig. 6c and d), precluding a simple AFC process. Furthermore, VBZ rocks display a puzzling decrease in MREE, HREE (e.g. Fig. 2e), and Nb/Ta ratios (Fig. 7a) with increasing SiO_2 contents. Correlations like these are a common feature of many rock suites emplaced throughout the TMVB (Luhr & Carmichael, 1985b; Verma, 1999, 2000b; Straub & Martin-Del Pozzo, 2001; LaGatta, 2003; Siebe et al., 2004; Schaaf et al., 2005). Fractional crystallization, with or without crustal assimilation, that involves the formation of a typical low-pressure mineral assemblage (Ol, Plag, Cpx and Opx) is unable to explain such trends because the HFSE and the REE are not significantly incorporated in these mineral species. Fractionation of Fe–Ti oxides from a basaltic magma will decrease the Nb and Ta contents of the derivative liquids, but it will also increase their Nb/Ta ratios because $D_{Nb}/D_{Ta} < 1$ in these phases (Green & Pearson, 1987).
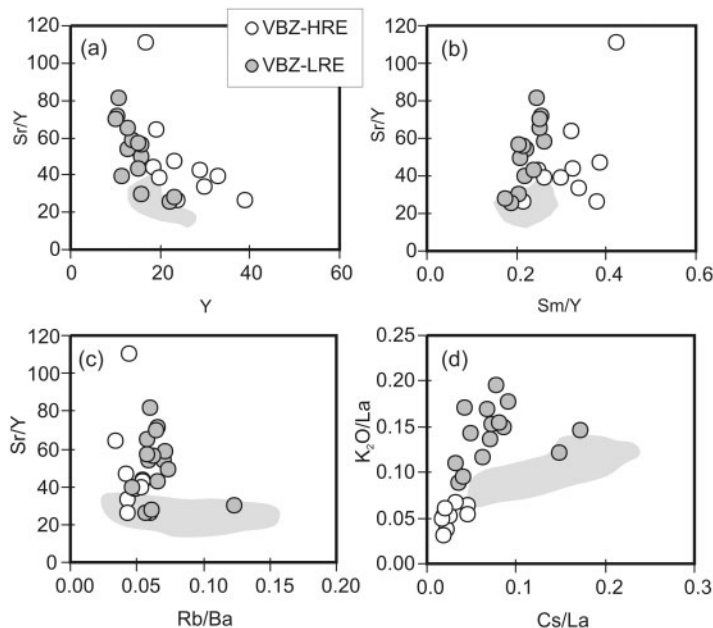
Fig. 4. Variation of (a) Sr/Y vs Y, (b) Sm/Y vs Sr/Y, (c) Rb/Ba vs Sr/Y, and (d) Cs/La vs K_2O/La compared with other Mexican volcanoes such as Popocatépetl (light grey field) at similar fractionation levels. Popocatépetl data from LaGatta (2003) and Schaaf *et al.* (2005).

It has also been proposed that amphibole fractionation at shallow levels (Castillo *et al.*, 1999), or fractionation of amphibole and garnet from hydrous basalts at high pressures (Müntener *et al.*, 2001), can explain the slab-melt geochemical features of some adakites (Castillo *et al.*, 1999; Garrison & Davidson, 2003; MacPherson *et al.*, 2006). Amphibole fractionation at either low or high pressures could in principle be responsible for the low MREE, Nb and Nb/Ta ratios in more evolved lavas, but in this case enormous quantities of fractionating amphibole (>85%) would be required to explain the observed variations (Fig. 7b and c). High-pressure fractionation experiments involving hydrous basalts essentially form residual websterites, with amphibole and garnet appearing at higher degrees of crystallization (Müntener *et al.*, 2001). High-pressure differentiation will also produce corundum-normative derivative liquids (Müntener *et al.*, 2001), and the strongest garnet signatures will probably be observed in the most evolved rocks (MacPherson *et al.*, 2006). Except for one relatively altered sample (ZIT-99-19), none of the VBZ rocks studied here are corundum normative. Furthermore, the strongest garnet signatures are observed in the relatively silica-poor VBZ-HRE (e.g. higher Sm/Y, Fig. 4b), in contrast to what would be expected if both suites were genetically related to deep crystal fractionation. In addition, even if a common parental basalt for the Mexican andesites exists at depth, the trace element and isotopic variations observed within the VBZ suite (Figs 3 and 5), and at different locations along the arc (Fig. 4), will be hard to explain by differentiation alone, and probably require a compositionally heterogeneous primary source.

In conclusion, although some fractionation and interaction with the continental crust is clearly unavoidable, as the magmas must traverse at least 30 km of continental crust before eruption, and there is unequivocal evidence of this interaction in the form of xenocrysts and xenoliths, the overall geochemical variations of the VBZ rock suites cannot easily be accounted for by crystal fractionation from a common primitive magma, nor by crustal assimilation or direct crustal anatexis; therefore, the following discussion assumes that their compositions largely represent mantle-derived and subduction-related phenomena.

Insights into the composition of the Mexican mantle wedge

The concentrations and ratios of the HFSE and the MREE–HREE are often used to infer the characteristics of the mantle source of arc lavas, because these elements are largely insoluble in aqueous fluids and thus are not significantly incorporated into the subduction flux (Class *et al.*, 2000; Hochstaedter *et al.*, 2001; Straub *et al.*, 2004; Pearce *et al.*, 2005). Based on this principle, arc magmas are generally considered to be derived from the partial fusion of a depleted N-MORB-like mantle source. In Mexico the composition of the pre-subduction mantle wedge is elusive because of the compositional heterogeneity of primitive basalts (Luhr & Carmichael, 1985a; Wallace & Carmichael, 1999; Verma, 2000b; Petrone *et al.*, 2003).
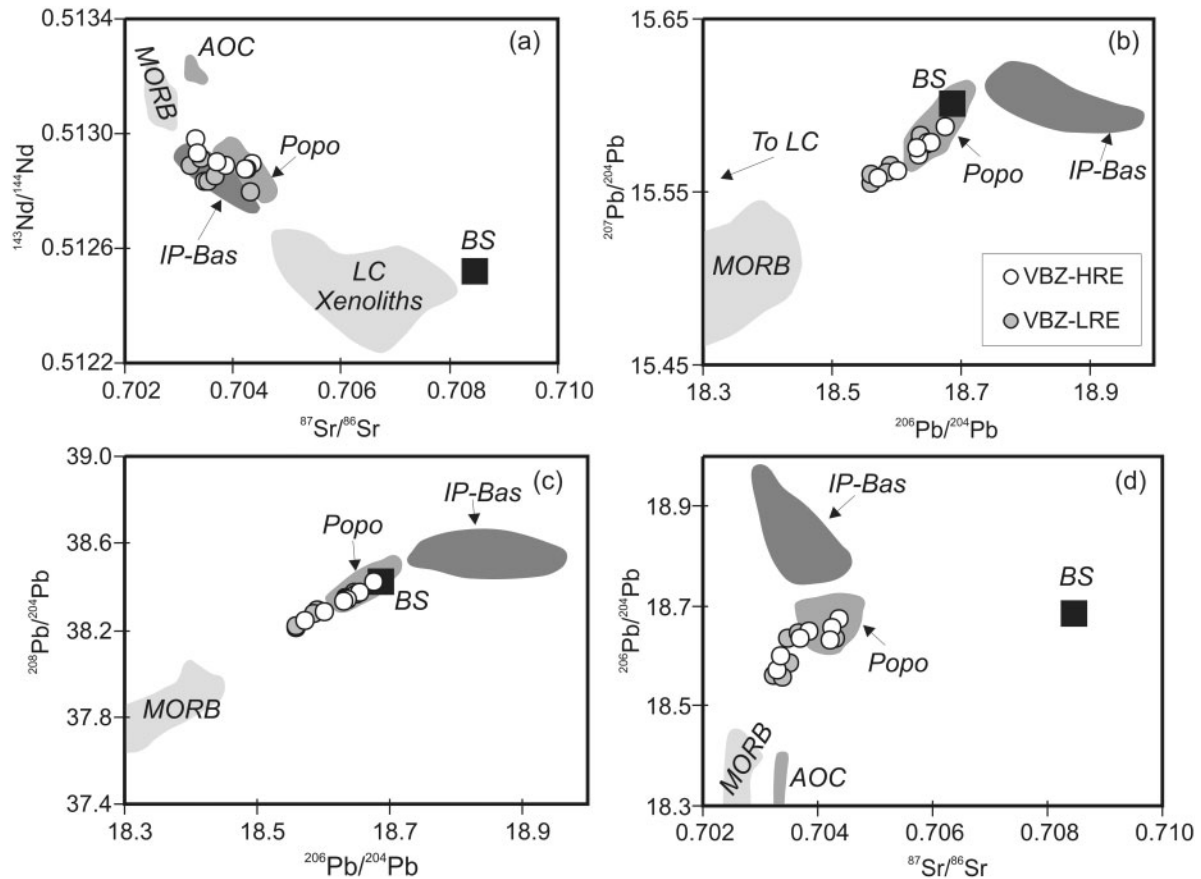
Fig. 5. Sr–Nd–Pb isotope variation diagrams for the studied rock suites and possible end-members. (a) $^{143}Nd/^{144}Nd$ vs $^{87}Sr/^{86}Sr$; (b, c) Pb isotope variation diagrams; (d) $^{206}Pb/^{204}Pb$ vs $^{87}Sr/^{86}Sr$. Also shown: data for 5–15°N East Pacific Rise MORB (MORB) [PETDB, 2006, http://www.petdb.org/(Lehnert *et al.*, 2000)]; weighted bulk sediment composition from DSDP Site 487 (BS) (Gómez-Tuena *et al.*, 2003; LaGatta, 2003); isotopic composition of the altered oceanic crust sampled at DSDP Site 478 (AOC) (Verma, 2000b); Sr–Nd composition of lower crustal xenoliths collected in northern Mexico (LC Xenoliths) (Ruiz *et al.*, 1988a, 1988b; Schaaf *et al.*, 1994); compositional field of 'intraplate' basalts (IP-Bas) from the Chichinautzin volcanic field (LaGatta, 2003) and the Palma Sola volcanic field (Gómez-Tuena *et al.*, 2003); compositional field of Popocatépetl stratovolcano (Popo) (LaGatta, 2003; Schaaf *et al.*, 2005).

Nonetheless, alkaline magmas with negligible subduction signatures and higher Nb contents and Nb/Ta ratios than MORB have been recognized all across the TMVB (Fig. 7). These rocks, often regarded as 'intraplate' or 'ocean island basalt (OIB)-like' magmas, also have isotopic compositions more 'enriched' than MORB (Verma, 2000b; Gómez-Tuena *et al.*, 2003; Petrone *et al.*, 2003). The presence of 'intraplate-like' rocks in close space–time association with more typical calc-alkaline arc volcanic rocks has been taken as indicating a highly heterogeneous mantle wedge in the Mexican subduction zone (Luhr & Carmichael, 1985a; Wallace & Carmichael, 1999; Verma, 2000b; Petrone *et al.*, 2003).

Some researchers have suggested that these enriched mantle domains could have been dragged from the back-arc region into the arc source by mantle convection and corner flow (Luhr & Carmichael, 1985a; Wallace & Carmichael, 1999). Others have considered the existence of a mantle plume (Márquez *et al.*, 1999), or association

with decompression melting by rifting (Verma, 2002). More recently, Ferrari (2004) suggested that these enriched mantle domains were probably infiltrated into the arc source region following a slab detachment event. However, regardless of the tectonic explanations that have been suggested for the existence of 'intraplate' rocks in the Mexican arc, their presence is often considered to be an anomaly that was somehow introduced into the more typical 'depleted mantle', because their volume is appreciably small when compared with the more abundant arc-related calc-alkaline sequences.

The decrease of HFSE and MREE–HREE contents, together with Nb/Ta ratios, with increasing SiO_2 contents (Fig. 7) is a puzzling characteristic that has been observed in many rock sequences emplaced all across the TMVB (Luhr & Carmichael, 1985b; Verma, 1999, 2000b; Straub & Martin-Del Pozzo, 2001; Siebe *et al.*, 2004; Schaaf *et al.*, 2005). Notably, intraplate volcanic rocks with negligible subduction signals often plot as an enriched
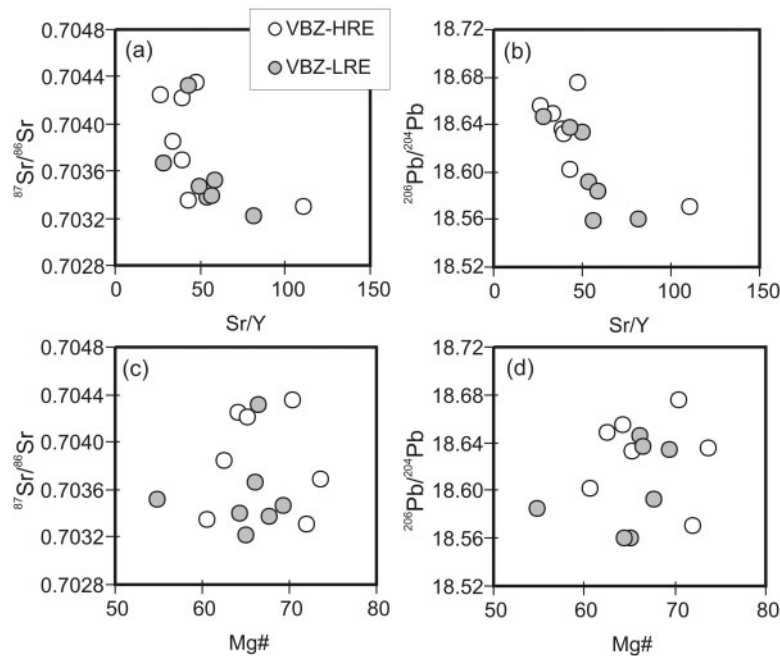
Fig. 6. Relationships between Mg-number, Sr/Y and Pb–Sr isotopic composition for VBZ rocks. Sr/Y ratios correlate inversely with (a) $^{87}Sr/^{86}Sr$ and (b) $^{206}Pb/^{204}Pb$, indicating that the slab-melt geochemical signal tends to have the isotopic characteristics of MORB. (c, d) Variation of $^{87}Sr/^{86}Sr$ and $^{206}Pb/^{204}Pb$ vs Mg-number. Calculated molar Mg-number $= Mg/(Mg + 0.85Fe^{2+}_{tot})$.

end-member in a continuum trend with the rest of the arc-like sequences (Fig. 7). As mentioned above, and as pointed out by previous workers, correlations like these cannot be easily accounted for by a simple liquid line of descent triggered by the crystallization of a typical mineral assemblage, at either low or high pressures, even one extensively modified by crustal assimilation (Fig. 7). In addition, Nb/Ta ratios should not be significantly fractionated by moderate to high extents of mantle melting, because partitioning between these elements and the dominant mantle mineralogy are very similar. Therefore the variations observed in Fig. 7 could, in principle, be attributed to the inherited compositional heterogeneity of the sub-arc mantle wedge beneath Mexico that has been fluxed to various extents by the subduction agents. This interpretation will also mean, however, that rocks with high SiO_2 contents may still represent direct mantle melts because Nb/Ta ratios correlate inversely with SiO_2, and this variation does not appear to be an artifact of fractionation or crustal contamination.

Water-saturated melting experiments on peridotite have been able to produce high-MgO andesites (Hirose, 1997), and experimental evidence of lavas from the VBZ (Blatter & Carmichael, 2001), together with the presence of amphibole-bearing peridotite nodules in at least one andesitic lava flow (Blatter & Carmichael, 1998*a*), appears to support the possibility of andesite formation by direct partial melting of the mantle. Nonetheless, to our knowledge, no hydrous melting experiment of peridotite has

produced melts with such high silica content as those observed here. The conundrum is thus clear: either there is a mechanism to form very high silica andesites by direct partial melting of the mantle, or the Nb/Ta ratios in this case are simply not reflecting the characteristics of the mantle source.

The usefulness of HFSE ratios as indicators of the mantle source in arc settings relies heavily on the assumption that these elements are not mobilized and/or fractionated by the subduction agents; that is, they behave as 'conservative' elements. Support for the insoluble nature of the HFSE in aqueous fluids is clearly established by the experimental evidence (McCulloch & Gamble, 1991; Brenan *et al.*, 1994, 1995*c*), and the relative low HFSE contents observed in arc rocks with large slab-derived fluid signatures alone (Straub *et al.*, 2004). Nonetheless it has also been increasingly recognized that the HFSE could be mobilized to some extent if the subduction component is in the form of a partial melt coming from the metamorphosed subducted basalt or its sedimentary cover (Stolz *et al.*, 1996; Bourdon *et al.*, 2002). The mobility of these elements, and the possibility to fractionate them, will depend on the residual mineral assembly of the partially melted slab. It has been long considered that rutile should be a residual phase during partial melting of the metamorphosed oceanic crust and sediments, because otherwise the typically high LILE/HFSE ratios observed in modern adakites and Archaean tonalite–trondhjemite–granodiorite (TTG) sequences could not be
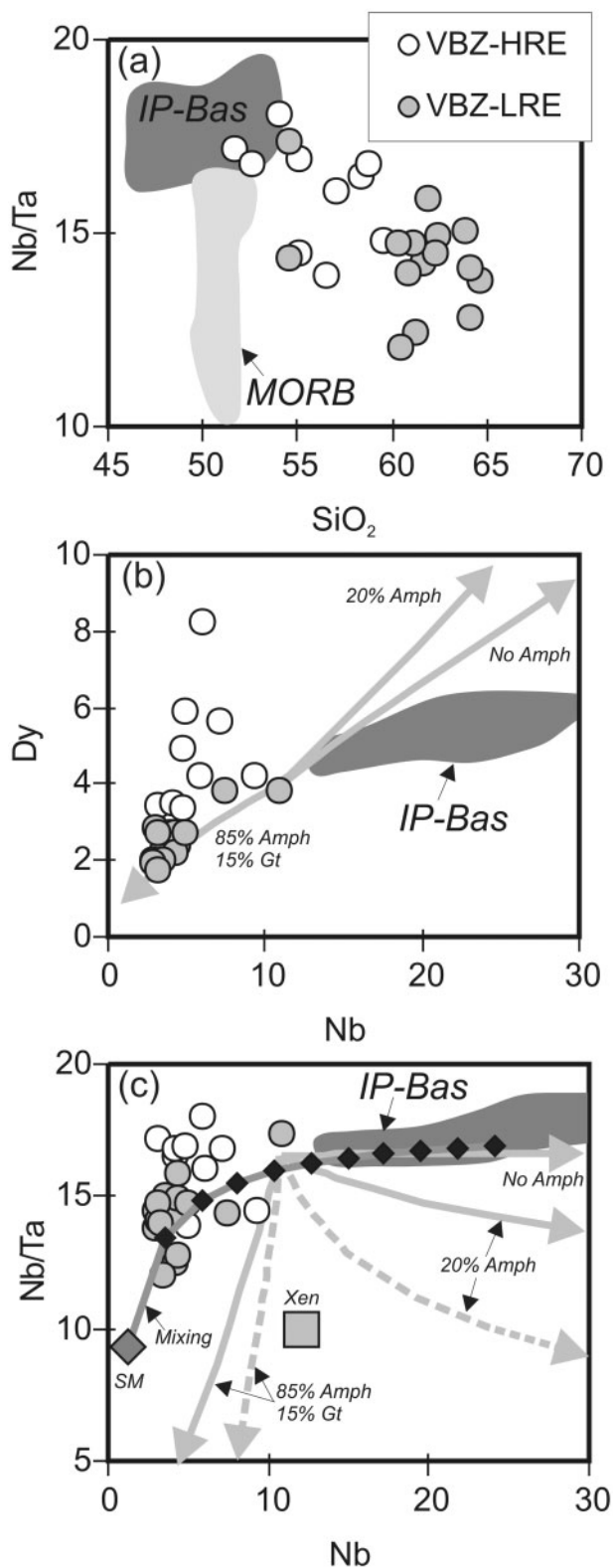
Fig. 7. Nb/Ta vs SiO$_2$ (a), Dy vs Nb (b) and Nb/Ta vs Nb (c) for VBZ rocks. High-SiO$_2$ andesites from the VBZ tend to have lower Nb/Ta ratios, MREE–HREE and Nb contents than true basalts from

preserved (Kelemen *et al.*, 2004). Nonetheless, experimental evidence indicates that rutile preferentially incorporates Ta over Nb ($D_{Nb}/D_{Ta} < 1$), so that high Nb/Ta ratios might be expected in the partial melts when a rutile-bearing residual assemblage is formed (Green, 1995; Schmidt *et al.*, 2004). In contrast, recently determined partition coefficients between these elements and low-MgO amphiboles indicate that $D_{Nb}/D_{Ta} > 1$, and therefore low Nb/Ta ratios might be expected in the slab-derived partial melts when amphibole remains in the residue and the melt fraction is low enough (Tiepolo *et al.*, 2000). Notably, even if some rocks with slab-melt geochemical characteristics have the high Nb/Ta ratios indicative of residual rutile (Stolz *et al.*, 1996; Gómez-Tuena *et al.*, 2003), the vast majority of the studied adakites, as well as the Archean TTG sequences and the bulk continental crust, display subchondritic Nb/Ta ratios (Foley *et al.*, 2002). This characteristic has been taken as evidence for the importance of residual amphibole during partial melting of the subducted slab (Foley *et al.*, 2002), although other investigators have argued that the low Nb/Ta ratios could still be formed with rutile-bearing eclogite residues if the original lithologies involved in the partial melting event had low Nb/Ta ratios to begin with (Rapp *et al.*, 2003).

Although the specific residual mineralogy involved during a slab melting event is hard to define, the experimental results provide insights into the origin and compositional characteristics of the mantle wedge and subduction

the TMVB. These variations are difficult to explain by crystal fractionation (or AFC) of a basaltic magma unless enormous quantities of fractionating amphibole are considered. Fractional crystallization and contamination models (continuous-line and dashed-line arrows, respectively) are shown with different proportions of fractionating amphibole. Models in (b) and (c) use an arc basalt from the Chichinautzin volcanic field as initial magma [sample 297 from Wallace & Carmichael (1999), further analyzed for trace elements by LaGatta (2003), with 10·74 ppm Nb, 0·648 ppm Ta and Nb/Ta = 16·57]. Contamination (AFC) models in (c) use a gneissic enclave (gray square, Xen) from the Chalcatzingo domes (A. Gómez-Tuena, unpublished data) located ~40 km SW of Popocatépetl volcano as contaminant (Nb 12·13 ppm, Ta 1·22 ppm, Nb/Ta = 9·9). Fractional crystallization models without amphibole use bulk $D_{Nb} = 0·014$, $D_{Ta} = 0·016$ and $D_{Dy} = 0·167$ (assuming fractionation of 35% Ol, 34% Cpx, 20% Opx, 10% Plag, 1% Fe–Ti oxides). Fractional crystallization and AFC ($M_a/M_c = 0·8$) models involving amphibole use $D_{Nb} = 0·338$, $D_{Ta} = 0·213$ and $D_{Dy} = 0·277$ (assuming 34% Ol, 20% Amph, 20% Opx, 15% Cpx, 10% Plag, 1% Fe–Ti oxides), and $D_{Nb} = 1·387$, $D_{Ta} = 0·852$ and $D_{Dy} = 1·235$ (assuming 85% Amph, 10% Gt). Also shown in (c) is a simple mixing model (line with black diamonds) of a slab melt (gray diamond, SM) calculated from the composition of the AOC at DSDP Site 487 (Nb 0·49 ppm, Ta 0·034 ppm, Nb/Ta = 14·5; see Table 4 for partition coefficients) and an 'intraplate' basalt from the Chichinautzin volcanic field [sample ASC44 from LaGatta (2003) with 24·08 ppm Nb, 1·427 ppm Ta and Nb/Ta = 16·9]. The analytical precision of the Nb/Ta ratios of repeated standards with similar concentrations to the samples is ~2·5% (2σ), similar to the size of the plotted symbols. Also included in (a) is the EPR-MORB field from Donnelly (2002).

components involved in the petrogenesis of the Mexican arc. The Nb/Ta variations (Fig. 7) might be explained if the slab-derived chemical flux affecting the arc source region is a water-rich silicate melt derived from the partial fusion of the subducted basalt and sediments, rather than an aqueous fluid in which the HFSE and the HREE are immobile. Low HFSE–HREE contents, together with low Nb/Ta ratios, strong subduction signatures and high SiO_2 contents, are all typical characteristics of experimental slab melts and adakites worldwide, and are consistent with melting of garnet amphibolite. These siliceous melts may either react or mix with mantle peridotite and/or their melts during ascent through the mantle and crust (Kelemen, 1998; Prouteau *et al.*, 2001; Tatsumi, 2001). Indeed, Fig. 7c shows that the Nb–Ta concentrations and ratios can be explained by mixing of a slab-derived silicate melt with an enriched 'intraplate' magma. The model uses the AOC (altered ocean crust) from DSDP Site 487 as a starting composition (Nb 0·49 ppm, Ta 0·034 ppm, Nb/Ta = 14·5), and assumes garnet amphibolite in the residue ($D_{Nb} = 0·775$ and $D_{Ta} = 0·555$; see Table 4) at 1% batch melting (AOC melt: Nb 0·63 ppm, Ta 0·0607, Nb/Ta = 10·4). Even though very low quantities of residual rutile (<1%) can significantly affect the Nb/Ta ratios of the resulting slab melt, and sediment contributions are not considered in this case, this exercise provides a feasible explanation for a typical geochemical feature displayed by several volcanic successions of the Mexican arc.

The above-mentioned hypothesis thus implies that the low HREE–HFSE contents and Nb/Ta ratios observed in the silica-rich calc-alkaline rocks could represent the inherited compositional characteristics of a slab-derived silicate melt that had a small contribution from the background mantle wedge (or its partial melts). The greater the interaction of the slab melts with the mantle wedge, or the higher the proportion of the 'intraplate' magmatic component in a possible magma mixing event, the larger the dilution effect of the slab-melt component in the resulting magmas. In this scenario, the enriched 'intraplate' basalts should best represent the composition of the pre-subduction background mantle wedge in Mexico. This will not imply, of course, that the mantle wedge below Mexico is compositionally homogeneous and identical to an OIB-like source. More research will be needed to test this hypothesis. However, the evidence does indicate that the geochemical tools that have proved useful in other arcs for identifying the composition of the mantle wedge are probably not applicable for the Mexican arc because the HFSE and the MREE–HREE have become an intrinsic ingredient of the subduction flux.

Subduction agents: the effect of AOC and sediment melts

As mentioned above, the VBZ rock suites display contrasting trace element patterns, slightly different isotopic compositions, and often follow diverging trends in several incompatible element ratio plots when compared with other Mexican volcanoes (Figs 3–5). If the geochemical compositions are not significantly controlled by crystal fractionation and/or additions from the continental crust, then one can safely assume that they are controlled by the contributions from the subducted slab and the mantle wedge.

Element ratios between Th, Pb, Nd and Sr are useful indicators of slab-derived chemical fluxes because the partitioning of these elements between slab-derived fluids or melts have been extensively studied (Defant & Drummond, 1990; Drummond & Defant, 1990; Brenan *et al.*, 1995*a*; Elliott *et al.*, 1997; Johnson & Plank, 1999; Class *et al.*, 2000; Foley *et al.*, 2002; Kessel *et al.*, 2005). Th and Nd are fluid immobile (Brenan *et al.*, 1994, 1995*c*; Stadler *et al.*, 1998; Kessel *et al.*, 2005), whereas Pb and Sr are soluble in aqueous fluids (Brenan *et al.*, 1994, 1995*c*; Keppler, 1996; Adam *et al.*, 1997; Ayers *et al.*, 1997; Stadler *et al.*, 1998; Kessel *et al.*, 2005). Therefore, Th and Nd budgets in arc magmas should be mainly controlled by their relative abundances in the mantle wedge plus the slab-melt additions (sediment + AOC). The Pb and Sr contributions, on the other hand, can be controlled by fluids and/or slab-melt additions to the mantle wedge because they are highly soluble, and fairly incompatible during partial melting of eclogite and amphibolite sources (Defant & Drummond, 1990; Tiepolo *et al.*, 2000; van Westrenen *et al.*, 2001; Barth *et al.*, 2002; Foley *et al.*, 2002; Kessel *et al.*, 2005). In addition, because the altered (or fresh) subducted oceanic crust and overlying sediments have different Sr, Nd and Pb isotopic compositions (Verma, 2000*b*; Gómez-Tuena *et al.*, 2003; LaGatta, 2003), the isotopic variations observed in the magmatic rocks can be used to differentiate between different fluids or melts originating from different portions of the subducted slab.

VBZ samples show a positive correlation between Th/Nd and Pb/Nd, indicating that Pb and Th are incorporated at a constant ratio in the subduction flux (Fig. 8a). The coupling of a fluid-mobile element (Pb) with an insoluble one (Th), and a correlation trending towards higher Th/Nd ratios than those of the subducted sediments, are indications that sediment additions into the mantle source are in the form of a silicate melt rather than an aqueous fluid. This interpretation is further confirmed in the rough but discernible negative correlation of Pb/Nd and Nd isotopes (Fig. 8b), a characteristic that has been often cited as indicating a sediment-melt component that contributes Th, Pb and unradiogenic Nd (Elliott *et al.*, 1997; Class *et al.*, 2000; Hochstaedter *et al.*, 2001; Gómez-Tuena *et al.*, 2003; Kelemen *et al.*, 2004). However, low Pb/Nd ratios extend to lower $^{143}Nd/^{144}Nd$ values (Fig. 8b) than the EPR-MORB, indicating that the

Table 4: End-member compositions and partition coefficients used in models

	Mantle wedge[1]	AOC[2]	Bulk sed.[3]	$D_{AOC/melt}$[4]	$D_{sed/melt}$[5]	$D_{mantle/melt}$[6]	AOC melt[7]	Sed. melt[8]
Rb	0·74	2·94	94·14	0·032	0·72	0·00010	71·11	128·26
Ba	8·32	8·66	2910	0·025	0·75	0·00011	248·38	3816·79
Th	0·09	0·10	6·70	0·067	0·89	0·00037	1·35	7·48
U	0·027	0·072	3·168	0·066	0·93	0·00110	0·96	3·39
Nb	1·26	1·77	9·71	0·775	1·21	0·00228 (0·212)	2·27	8·10
Ta	0·075	0·108	0·673	0·555	1·2	0·00288 (0·243)	0·19	0·57
La	1·22	2·00	39·31	0·265	1·34	0·00552	7·35	29·71
Ce	2·81	6·21	48·83	0·380	1·35	0·00819	16·07	36·64
Sr	30·92	140·00	231·40	0·122	0·51	0·01704	1070·50	432·94
Pb	0·15	0·26	41·36	0·123	1·29	0·02269	2·01	32·43
Nd	2·02	6·38	37·68	0·599	1·53	0·02253	10·58	25·06
Sm	0·54	2·40	7·78	0·924	1·6	0·03672	2·59	4·95
Zr	14·05	56·85	107·78	0·423	1·64	0·02332 (0·083)	132·74	67·03
Hf	0·45	1·73	2·42	0·567	1·64	0·03532 (0·095)	3·02	1·50
Eu	0·20	0·90	2·06	1·400	1·68	0·05000	0·64	1·25
Gd	0·63	3·65	8·32	1·880	1·65	0·05897	1·95	5·14
Tb	0·11	0·68	1·31	2·730	1·66	0·07876	0·25	0·81
Dy	0·65	4·51	7·75	4·140	1·68	0·09666	1·10	4·71
Y	3·74	27·35	49·15	4·750	1·69	0·11038	5·80	29·69
Ho	0·13	1·00	1·63	5·355	1·69	0·11667	0·19	0·99
Er	0·39	2·84	4·55	5·720	1·69	0·13486	0·50	2·75
Yb	0·37	2·66	4·28	6·770	1·68	0·15196	0·40	2·60
Lu	0·06	0·41	0·69	9·162	1·72	0·16238	0·04	0·41
$^{87}Sr/^{86}Sr$	0·702900	0·702900	0·708458				0·702900	0·708458
$^{206}Pb/^{204}Pb$	18·680	18·271	18·687				18·271	18·687
$^{207}Pb/^{204}Pb$	15·580	15·489	15·601				15·489	15·601
$^{208}Pb/^{204}Pb$	38·400	37·748	38·423				37·748	38·423
$^{143}Nd/^{144}Nd$	0·513010	0·513160	0·512518				0·513160	0·512518

[1]Mantle wedge composition is sample ASC44 from the Chichinatzin volcanic field (LaGatta, 2003) inverted at 5% batch melting to a spinel peridotite (53% Ol, 17% Cpx, 28% Opx, 2% Sp). Individual mineral K_d values from Hart & Dunn (1993), Kelemen *et al.* (1993), Johnson (1994), Salters & Longhi (1999) and Donnelly (2002).
[2]Altered oceanic crust composition is a mixture of 80% AOC from DSDP Site 487 (Verma, 2000*b*; LaGatta, 2003) and 20% of an average fresh EPR-MORB between 5° and 15°N from the PETDB database (http://www.petdb.org/) with slightly higher Sr contents and $^{87}Sr/^{86}Sr$ ratios to account for alteration.
[3]Bulk sediment composition from DSDP Site 487 from LaGatta (2003) and Gómez-Tuena *et al.* (2003).
[4]Bulk solid–melt partition coefficients of andesitic–dacitic melts in equilibrium with a garnet amphibolite residuum (30% Cpx, 30% Gt, 40% Amph). Individual mineral K_d values from Rollinson (1993, and references therein), Green (1995), Tiepolo *et al.* (2000), van Westrenen *et al.* (2001), Barth *et al.* (2002) and the Geochemical Earth Reference Model (GERM) (http://www.earthref.org).
[5]Bulk solid–melt partition coefficients for sediment melting from Johnson & Plank (1999), except for Zr and Hf, which are extrapolations.
[6]Bulk solid–melt partition coefficients for a metasomatized mantle wedge assuming a residual mantle mineralogy made of 54% Ol, 10% Cpx, 34% Opx, 2% Gt. Bulk *D* values for HFSE assuming 0·3% residual rutile are shown in parentheses. Rutile $K_{d\ Nb} = 70$, $K_{d\ Ta} = 80$, $K_{d\ Zr} = D_{Hf} = 20$ are best-fit values based on Foley *et al.* (2000) and Schmidt *et al.* (2004).
[7]Composition of an AOC melt assuming 1% batch melting.
[8]Composition of a sediment melt assuming 5% batch melting.

mantle wedge component contributing to the magmas has to be more isotopically enriched (i.e. lower $^{143}Nd/^{144}Nd$) than the EPR-MORB source, and more similar to 'OIB-like' intraplate basalts.

The simple scenario of sediment-melt additions into an enriched mantle wedge is further complicated when the contribution of Sr, and the isotopic compositions of Sr and Pb, are taken into account. Figure 8c shows that
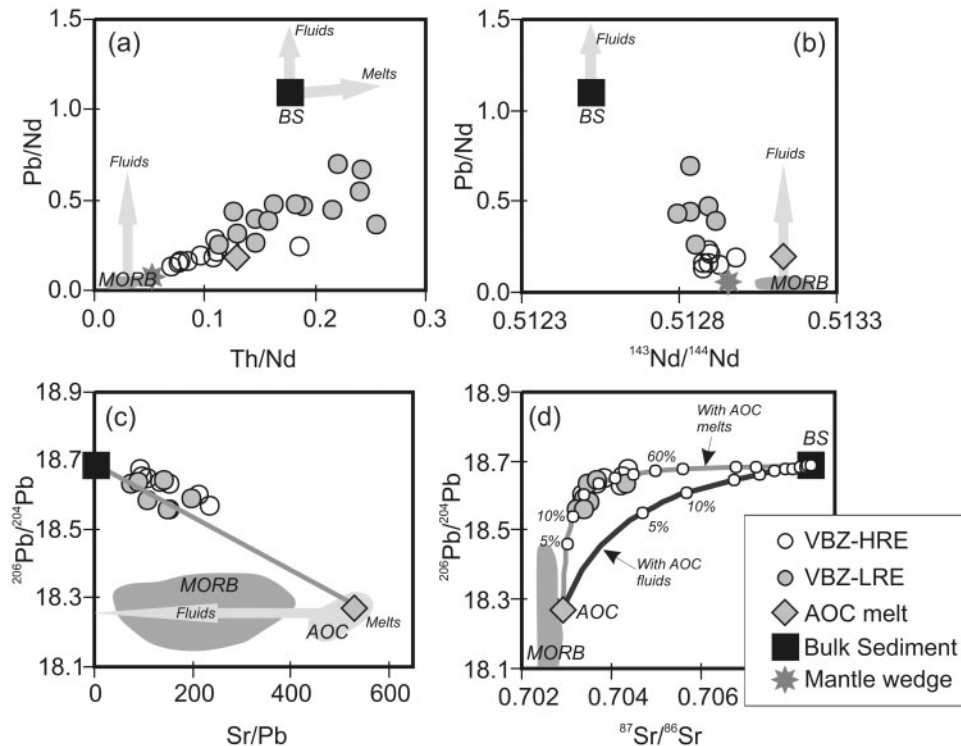
Fig. 8. Identification of subduction components in the VBZ rocks. (a) Pb/Nd ratios correlate positively with Th/Nd values, and (b) inversely with $^{143}Nd/^{144}Nd$ isotopes. These suggest the addition of a sediment partial melt to an isotopically enriched mantle wedge. (c) Sr/Pb ratios define a negative correlation with $^{206}Pb/^{204}Pb$ that projects towards the composition of the AOC. As Pb is significantly more incompatible than Sr in aqueous fluids, and both elements become similarly incompatible only during partial melting (Kessel *et al.*, 2005), the high Sr/Pb component is consistent with a melt derived from the AOC. (d) The Sr–Pb isotopic variation of the VBZ can be explained by mixing different proportions of melts from the subducted slab (sediments and AOC), but cannot be reproduced if the AOC component is considered to be an aqueous fluid. AOC and bulk sediment compositions, as well as slab-melt partition coefficients, are shown in Table 4. The AOC fluid was calculated assuming 1% fluid release (Sr 48·1 ppm, Pb 0·835 ppm, Sr/Pb = 57·55) using the partition coefficients reported by Kessel *et al.* (2005) for fluids in equilibrium with an eclogite residuum at 700°C ($D_{Sr} = 2·93$ and $D_{Pb} = 0·3l$).

the VBZ rocks form an inverse correlation between Sr/Pb and Pb isotope ratios that trend toward a DSDP Site 487 sediment end-member with high Pb isotope ratios on one hand, but whose other end-member is an isotopically depleted (low Pb isotope ratio) MORB-like component with Sr/Pb ratios that are higher than EPR-MORB. This component is different from what would be expected from an aqueous fluid derived from the dehydration of AOC, but is consistent with a silicate melt derived from its partial fusion. Although Pb and Sr are soluble elements, experimental data indicate that Pb is significantly more incompatible than Sr in aqueous fluids extracted from a plagioclase-free source, and that it is only when partial melting is achieved that Sr and Pb are incorporated in the melt at similar rate (Brenan *et al.*, l995*b*, l995*c*; Kessel *et al.*, 2005). Supercritical fluids will preferentially incorporate Sr over Pb, but this will only happen at much higher pressures (Kessel *et al.*, 2005). In addition, Fig. 8d shows that MORB or AOC, bulk Site 487 sediment, and the VBZ data form a hyperbolic trend for Sr–Pb isotope ratios that is consistent with binary mixing. The curvature of the trend can only be reproduced if the depleted

MORB-like component is a partial melt with a relatively higher Sr/Pb ratio than that of a fluid extracted from the same source.

Modeling subduction and mantle contributions

Figure 8 shows that the overall compositions of the studied rock suites can be explained by mixing of two chemically distinct subduction components derived from the partial fusion of the subducted sediments and underlying oceanic crust. Participation of an enriched mantle wedge, with lower Nd isotope ratios than EPR-MORB, is also apparent from Fig. 8b. Although the precise chemical compositions of these end-members are difficult to constrain, they can be calculated to a reasonable extent with the geological and compositional information available (Table 4).

We have shown above that the entire trace element budget of the VBZ rocks could have been affected by contributions from the subducted slab. This complicates calculation of the composition of the background mantle wedge in the region. Nonetheless, the data indicate that its

composition is more similar to the enriched OIB-like mantle that gives rise to the Mexican intraplate basalts than to the source of EPR-MORB (Figs 7 and 8). For this reason, we calculated the trace element composition of the mantle wedge component by inverting the trace element contents of a MgO-rich basalt from the Chichinautzin volcanic field (Wallace & Carmichael, 1999) that shows very little indication of a subduction-derived component (Table 4). The concentrations of Ba, Pb and Sr in the original sample were slightly reduced to have a smooth trace element pattern in a MORB-normalized trace element variation diagram, but no further corrections were made to account for fractionation. We thus emphasize that the modeled slab contributions to the calculated mantle wedge should be considered as maxima in this case. The Nd isotopic composition of the mantle $(^{143}Nd/^{144}Nd = 0.51301)$ was calculated by extrapolation of the trend observed in Fig. 8b, and is similar to that observed in intraplate basalts from other parts of Mexico (Luhr et al., 1989; Pier et al., 1989; Wallace & Carmichael, 1999; Lassiter & Luhr, 2001; Gómez-Tuena et al., 2003; LaGatta, 2003; Petrone et al., 2003). Because the Pb and Sr isotopic compositions of the studied rock suites are strongly controlled by the slab-derived agents (Fig. 8d), the values for the mantle wedge were assumed to be slightly more enriched than the average EPR-MORB $(^{87}Sr/^{86}Sr = 0.7029$, $^{206}Pb/^{204}Pb = 18.68$, $^{207}Pb/^{204}Pb = 15.58$, $^{208}Pb/^{204}Pb = 38.40)$, and are also similar to the values observed in Mexican intraplate basalts (Table 4).

The composition of the sediment melt was calculated using the weighted bulk sediment composition from DSDP Site 487 (Gómez-Tuena et al., 2003; LaGatta, 2003) and assuming 5% batch melting, using the partition coefficients reported by Johnson & Plank (1999) (Table 4). The models consider no major changes in fluid-mobile element contents during fore-arc devolatilization, and assume that melting of the bulk subducted sediment occurs at arc front depths.

A major uncertainty in this modeling is the composition of the altered oceanic crust. The AOC at DSDP Site 487 (Verma, 2000b) is an obvious possibility; however, these particular samples have extremely depleted REE patterns and higher $^{143}Nd/^{144}Nd$ ratios when compared with most East Pacific Rise samples [PETDB: Petrological Database of the Ocean Floor, 2006, http://www.petdb.org/(Lehnert et al., 2000)]. Therefore, it is unclear to what extent the Site 487 AOC samples represent the bulk oceanic crust that is being subducted along the Middle American Trench (Gómez-Tuena et al., 2003). Nonetheless, if an average composition of a fresh EPR-MORB is chosen as the starting material, then there will be a large uncertainty on the amount of alteration and mobility of key elements that might be transferred to the arc source region during subduction. For these reasons,

the models below use both the composition of the pristine AOC at DSDP Site 487 and a hypothetical AOC calculated by mixing 20% of an average EPR-MORB with the DSDP 487 AOC (Table 4). The compositions of the AOC melts were calculated using the average and/or best-fit partition coefficients of andesitic and dacitic liquids, and assuming 1% batch melting with a garnet amphibolite residuum (Table 4).

Natural and experimental slab melts are not in equilibrium with mantle olivine and should react with mantle peridotite during ascent (Rapp et al., 1999). Various experiments and models indicate that slab-melt–peridotite interaction forms Opx-rich lithologies at the expense of olivine, but other phases have also been identified: Al-augite, garnet, plagioclase and hydrous minerals such as amphibole and/or phlogopite (Kelemen, 1998; Prouteau et al., 1999; Rapp et al., 1999; Tatsumi & Hanyu, 2003; Kelemen et al., 2004). Thus modeling such a reaction strongly depends on the partition coefficients between trace elements and the mineral species that are consumed and created. Some workers have attempted to model these reactions using the AFC formulation of DePaolo (1981), and assuming that the slab melts heat as they rise and decompress while assimilating mantle peridotite (Tatsumi & Hanyu, 2003; Kelemen et al., 2004). Others have modeled the process using a simple mixing approach, considering that small amounts of slab-derived additions will not have a significant effect in modifying the mantle mineral paragenesis (Elliott et al., 1997; Class et al., 2000; Gómez-Tuena et al., 2003). Both kinds of models, although conceptually distinct, tend to provide similar results because the incompatible trace element patterns will be essentially governed by the slab-melt additions and the amount of mantle that could be assimilated or mixed.

Given the large uncertainty in the amount and compositions of the minerals that could be consumed and precipitated during melt–peridotite interaction, we have chosen to use the simple mixing approach. Nonetheless, we acknowledge that the ability for a slab melt to remain liquid during ascent will depend on the so-called 'effective' melt/peridotite ratio (Rapp et al., 1999). If this ratio remains high, then slab melts could escape significant modification of their incompatible element contents (Rapp et al., 1999). Relatively high bulk Mg-number and Ni for given SiO_2 (see Fig. 2c) will probably be the only reliable indicators of slab-derived andesitic–dacitic melts interacting with the mantle wedge (Kelemen et al., 2003; Kessel et al., 2005). In contrast, if the melt/peridotite ratio is relatively low, then melts could solidify completely and form a modally metasomatized, Opx-rich, hybrid mantle that could be later remelted during decompression and ascent. As the partition coefficients for Opx and Ol and most of the elements considered here are extremely
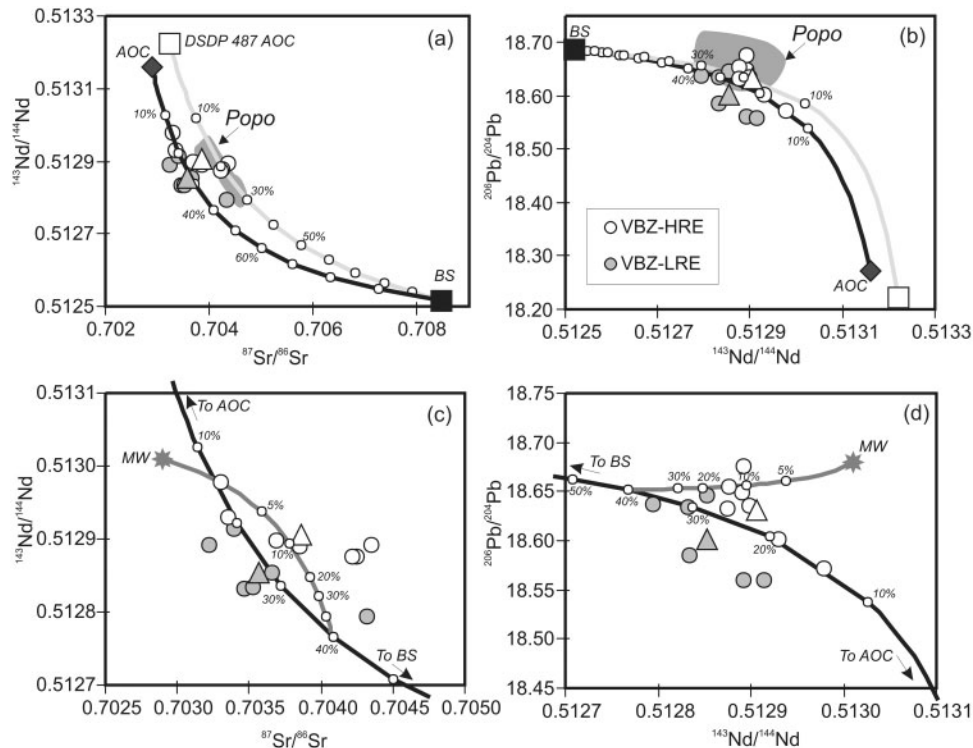
Fig. 9. Simple mixing modeling results of slab-melt–mantle interactions for the studied rock suites in (a) Sr–Nd and (b) Pb–Nd isotopic space. A mixing model that uses the DSDP 487 AOC can explain, to a large extent, the compositions of the volcanic products of Popocatépetl stratovolcano (Popo) but is unable to explain the compositions of the VBZ suite. Thus a slightly different AOC was constructed to account for the discrepancy (Table 4). The VBZ-LRE rocks are interpreted to be slab melts with little mantle contribution, and with isotopic compositions that reflect variable proportions of sediment and AOC melts. An average VBZ-LRE (large filled triangle) can be formed by a mixture of ∼ 70% AOC melt and ∼30% sediment melt. (c) and (d) show modeling results of slab-melt additions to the mantle wedge (MW). Adding ∼10% of a bulk slab component (made of 60% AOC and 40% sediment melt) into the calculated mantle wedge can closely reproduce the isotopic composition of an average VBZ-HRE rock (△).

low, then moderate to large extents of melting of such a metasomatized mantle will not significantly change the trace element patterns of the resulting melts, and they will be similar to the composition of the bulk slab component itself, unless the proportions of accessory mineral phases such as amphibole, phlogopite or rutile are significantly large. The absolute concentrations, on the other hand, will be controlled by the slab-melt/peridotite ratio, the residual mineralogy, and the extent of melting.

Modeling results

Figure 9 shows modeling results for slab-melt and mantle interactions in Sr, Nd and Pb isotopic variation diagrams. If a melt of the AOC sampled at DSDP Site 487 is used as the depleted MORB-like component, the mixing line in Sr–Nd isotopic space (Fig. 9a) passes over the isotopic compositions of Popocatépetl volcano but is largely unable to reproduce the VBZ data. This probably indicates that the AOC component contributing to VBZ has a slightly different composition from the one contributing to Popocatépetl. For this reason, we slightly adapted the AOC isotopic compositions to fit the observed VBZ

geochemical trends, while keeping the bulk-sediment constituent fixed. The isotopic values for this new 'AOC' are within the range of those observed in EPR-MORB for Pb and Nd but have a slightly higher $^{87}Sr/^{86}Sr$ ratio and Sr contents to account for alteration. The rest of the trace elements represent a mixture of 80% AOC from DSDP Site 487 and 20% of an average fresh sample from the EPR (Table 4).

By using this hypothetical AOC the VBZ-LRE rock suite samples plot within a mixture made of 80:20 and 60:40 AOC melt:sediment melt (Fig. 9). An average VBZ-LRE rock could be explained by a mixture of about 70:30 AOC melt:sediment melt (large filled triangle in Fig. 9), with very little contribution from the mantle wedge. The trace element pattern of such a mixture is very similar to an average VBZ-LRE rock, except for the fluid-mobile elements (Rb, Ba, U and Pb) (Fig. 10a). Several possible explanations can account for these differences. They might reflect the above-mentioned uncertainty in the composition of the AOC that is being subducted, or it could be that some of these elements have been retained in hidden accessory mineral
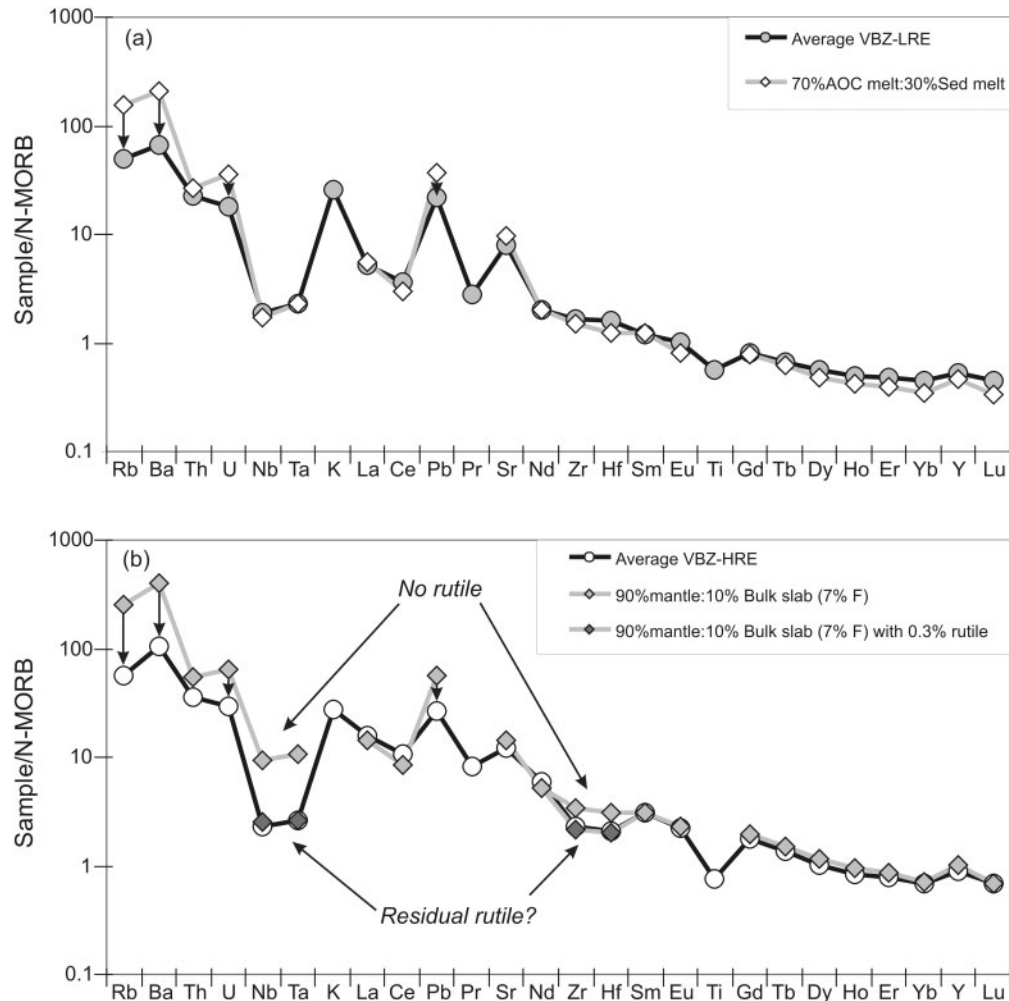
Fig. 10. (a) Model N-MORB-normalized trace element pattern compared with an average VBZ-LRE rock. The trace element pattern of an average VBZ-LRE rock is closely matched by a mixture of 70% AOC melt and 30% sediment melt, except for the fluid mobile elements. This suggests that these elements were either retained in an accessory residual phase or, more probably, released in a fluid phase before melting was achieved. (b) Model N-MORB-normalized trace element patterns show that most of the trace elements of an average VBZ-HRE can be reproduced by batch melting ($\sim$7% F) of a mantle wedge that has been metasomatized with $\sim$10% slab melt composed of 60% AOC and 40% sediment, except for the fluid-mobile elements and the HFSE. Even though the fluid-mobile element difference can be explained by retention or fluid release, the strong negative Nb–Ta and Zr–Hf anomalies probably necessitate the participation of $\sim$0·3% residual rutile in the mantle wedge (see text and Table 4 for modeling parameters).

phases that were not considered in the models, such as residual mica [e.g. Elburg *et al.* (2002)]. Nonetheless, the remarkable match in the rest of the elements, and the fact that the discrepancy affects only the most fluid-mobile elements, makes these interpretations unlikely. We consider it a more plausible explanation that a portion of these highly soluble elements has been simply lost in a fluid phase prior to melting at arc-front depths. This is conceivable because the solidus temperatures of wet basalt or sediments are significantly higher than the stability field of several of the hydrated mineral species that become unstable at relatively low metamorphic grades during subduction (Johnson & Plank, 1999; Poli & Schmidt, 2002). Thus, it seems inevitable that fluid

release from the subducted slab should precede anatexis. As the slab component contributing to VBZ-LRE is clearly a composite, it is difficult to quantify precisely the extent of element retention or depletion that affected the sediments and/or the altered oceanic crust. Nevertheless, if the modeled VBZ lavas are true liquid compositions, as previously indicated by the experimental evidence (Blatter & Carmichael, 2001), or have undergone a small amount of fractionation or trace element dilution during mantle interaction, then $\sim$66% of the Rb, $\sim$65% of the Ba, $\sim$50% of the U and $\sim$40% of the Pb must have been removed (or retained) from the available fluid-mobile element budget before being incorporated into the calculated bulk-slab component.

The VBZ-HRE rocks tend to have higher MgO and Ni contents, more radiogenic Nd isotope compositions, and lower Ba/La, Th/Nd and Pb/Nd ratios than the VBZ-LRE suite, features that are all indicative of a relatively higher contribution from the mantle wedge (Fig. 8). Figures 9c and d shows the effects of mixing a bulk-slab component (made of 60:40 AOC melt:sediment melt) into the calculated mantle wedge. The proportion of slab component needed to reproduce the isotopic compositions of an average VBZ-HRE rock can be constrained to be ~10%. Batch melting of such a metasomatized mantle (90% mantle: 10% slab-melt component) can reproduce fairly well the overall trace element patterns of an average VBZ-HRE rock if the fluid-mobile element contents of the bulk slab are adapted for depletion (or retention) in the proportions described above (Fig. 10b). Nevertheless, a model that assumes a peridotitic (or even pyroxenitic) residual mantle mineralogy is unable to reproduce the strong negative Nb–Ta and Zr–Hf anomalies of the VBZ-HRE rock suite because the partitioning of the HFSE and their neighboring elements in the normalized trace element diagrams are considered to be very similar. The HFSE should remain unaffected during the fluid loss that could have affected the LILE because these elements are insoluble in aqueous fluids. In addition, even though negative Zr–Hf anomalies are a common feature of sediments at DSDP Site 487, and are especially strong in the lower pelagic (non-terrigenous) section of the column, these sediments also have MORB-like Pb isotopic compositions (LaGatta, 2003), and their preferential incorporation into the VBZ-HRE magmas should be evident in plots involving Pb isotopes. As the VBZ-LRE and VBZ-HRE rocks are practically indistinguishable in their Pb isotopic compositions, the origin of the Zr–Hf anomalies observed in the VBZ-HRE cannot be related to the preferential incorporation of DSDP Site 487 pelagic sediments.

The presence of residual amphibole and/or rutile is often considered to play a significant role in the formation of Nb–Ta anomalies in slab-derived melts, but very little has been written about the effect on Zr and Hf. As mentioned before, the low Nb/Ta contents and ratios of the VBZ-LRE probably derive from the effect of residual amphibole during slab melting, but this same mineral has also been used to explain the absence of fractionation between Zr–Hf and the REE, because low-Mg amphibole favors the MREE over Zr and Hf (Foley *et al.*, 2002). At first sight it might appear that a different residual mineralogy involving rutile (or zircon) during slab melting explains the negative Zr–Hf anomalies observed in the VBZ-HRE suite. In detail, however, this is not sufficient to elucidate why these rocks appear to have a higher contribution from the mantle wedge, or why

those more likely representatives of pristine slab melts (the VBZ-LRE) do not display negative Zr–Hf anomalies.

A possible solution to this dilemma is that the Zr–Hf anomalies have been formed during partial fusion of a parcel of mantle that has been intensively modified by the addition of slab-derived silicate melts. Indeed, if slab melting does take place, then strong reaction of these melts with the surrounding mantle will occur unless the melt/peridotite ratio remains high (Rapp *et al.*, 1999). If the effective melt/peridotite ratio of an average VBZ-HRE magma is assumed to be as low as that constrained by the isotope diagrams (90% mantle: 10% slab melt), then it is very likely that the slab-derived melts were readily consumed and transformed into pyroxene-rich metasomatic lithologies. If these veins were later remelted in the presence of a residual accessory phase (e.g. rutile or zircon), the resulting magmas will display trace element patterns with unusual anomalies in those elements that became more compatible. In fact, Fig. 10b shows that a very small amount of residual rutile (~0·3%) during partial melting of such a modally metasomatized mantle can account for the strong Nb–Ta and Zr–Hf negative anomalies that are characteristic of the VBZ-HRE rocks. This could also explain the relatively high Nb/Ta ratios of the VBZ-HRE suite at relatively low Nb contents (Fig. 7).

A question that remains is whether an accessory titaniferous phase such as rutile can precipitate and remain stable in the mantle wedge after a partial melting event. Experimental studies and calculations have shown that rutile is not a likely residual phase in the source of basaltic melts, as the TiO_2 contents in basalts are too low (Green & Pearson, 1986; Ryerson & Watson, 1987); however, other studies have indicated that rutile could become stable in peridotite–melt systems under hydrous, silica-rich conditions (Schiano *et al.*, 1994, 1995; Bodinier *et al.*, 1995). In addition, accessory rutiles have also been directly observed and analyzed in modally metasomatized peridotites from Siberia (Ionov *et al.*, 1999; Kalfoun *et al.*, 2002). These studies have shown that rutile could become an important HFSE-bearing phase at least in the conditions of the upper mantle, and thus provide independent support for the presence of residual rutile during partial melting of a modally metasomatized mantle wedge.

CONCLUSIONS AND IMPLICATIONS

The geochemical data and modeling results provided here indicate that slab melting plays a key role in the petrogenesis of andesitic rocks of Valle de Bravo–Zitácuaro, in the central Trans-Mexican Volcanic Belt. Although these

magmas have traversed a 30–40 km thick continental crust, the geochemical results do not support simple crystal fractionation or crustal contamination as the main petrogenetic processes. Instead, the geochemical variations within the studied rock suites can be largely attributed to contribution of partial melts derived from the subducted basalt and its overlying veneer of sediment interacting with the mantle wedge. The new geochemical evidence thus supports previous experimental studies that suggested a mantle origin for andesites in the TMVB (Blatter & Carmichael, 2001; Carmichael, 2002). Nonetheless, the new data further suggest that a slab-derived siliceous melt interacting with the mantle wedge is probably a more effective mechanism to form high-SiO$_2$ andesites than water-saturated partial melting of the upper mantle.

The recognition that slab melting plays an important role in the Mexican arc, together with the conspicuous presence all across Mexico of 'intraplate' magmas with enriched (low Nd, high Sr, Pb) isotope ratios, yields a new perspective on the chemical character of the Mexican mantle wedge. Indeed, the results presented here indicate that the HFSE do not remain immobile during slab melting, and thus their concentrations and ratios in subduction-related lavas do not necessarily resemble those of the mantle source. Instead, the depleted mantle signatures (i.e. the low Nb/Ta ratios), together with strong subduction signals and high SiO$_2$ contents, could reflect the inherited character of the slab-melt component itself.

The models provided here also support results from experimental petrology (Johnson & Plank, 1999; Poli & Schmidt, 2002) indicating that the composition of subducted slabs changes during their journey into the mantle, and that they undergo intense modifications of their water content and fluid-mobile element budget as a result of continuous fluid release. In turn, we can distinguish the effects of different mechanisms of element recycling (hydrous fluids vs silicate melts) in the geochemistry of arc magmas because they imprint different geochemical characteristics on the volcanic products. Furthermore, because these differences should be ultimately linked to variations in P–T gradients, they provide an insight into the thermal and tectonic structure of a subduction zone. For instance, the low Nb/Ta ratios of the VBZ-LRE rocks indicate that slab melting probably occurred in the presence of amphibole, independently constraining slab depth to $\sim$75 km, equivalent to $<$25 kbar, because amphibole is unstable at higher pressures (Schmidt & Poli, 1998). If true, then it is possible that the Cocos slab remains flat for a longer distance, and melts at a significantly shallower depth than the hypothetical $\sim$100 km below the central part of the arc (Pardo & Suárez, 1995). A detailed seismic tomography

of central Mexico would be capable of testing this hypothesis.

Slab-melt–peridotite reactions also appear to be viable mechanisms for the formation of accessory mineral assemblages in the mantle wedge. As silicate melts are about 10 times more effective as metasomatic agents to form hydrous minerals than aqueous fluids (Schneider & Eggler, 1986), it does not seem surprising that the only reported locality in Mexico with amphibole-bearing lherzolites is the VBZ (Blatter & Carmichael, 1998a), and that their host is a VBZ-HRE rock (our sample ZIT-99-10). The presence of residual accessory phases such as amphibole, phlogopite or even rutile not only can selectively imprint unusual geochemical signals on the arc magmas, but could also represent important carriers of key trace elements in the convecting mantle to the temperatures and pressures at which they remain stable.

REFERENCES

Adam, J., Green, T. H., Sie, S. & Ryan, C. (1997). Trace element partitioning between aqueous fluids, silicate melts and minerals. *European Journal of Mineralogy* **9**, 569–584.

Atherton, M. & Petford, N. (1993). Generation of sodium-rich magmas from newly underplated basaltic crust. *Nature* **362**, 144–146.

Ayers, J., Dittmer, S. & Layne, G. (1997). Partitioning of elements between silicate melt and H$_2$O–NaCl fluids at 1·5 and 2·0 GPa pressure; implications for mantle metasomatism. *Geochimica et Cosmochimica Acta* **59**, 4237–4246.

Barth, M., Foley, S. & Horn, I. (2002). Partial melting in Archean subduction zones: constraints from experimentally determined trace element partition coefficients between eclogitic minerals and tonalitic melts under upper mantle conditions. *Precambrian Research* **113**, 323–340.

Blatter, D. & Carmichael, I. (1998a). Hornblende peridotite xenoliths from central Mexico reveal the highly oxidized nature of subarc upper mantle. *Geology* **26**, 1035–1038.

Blatter, D. & Carmichael, I. (1998b). Plagioclase-free andesites from Zitácuaro (Michoacán), México: petrology and experimental constraints. *Contributions to Mineralogy and Petrology* **132**, 121–138.

Blatter, D. & Carmichael, I. (2001). Hydrous phase equilibria of a Mexican high-silica andesite: a candidate for mantle origin? *Geochimica et Cosmochimica Acta* **65**, 4043–4065.

Blatter, D., Carmichael, I., Deino, A. & Renne, P. (2001). Neogene volcanism at the front of the central Mexican volcanic belt: basaltic andesites to dacites, with contemporaneous shoshonites and high-TiO$_2$ lava. *Geological Society of America Bulletin* **113**, 1324–1342.

Bodinier, J., Merlet, C., Bedini, R., Simien, F., Remaidi, M. & Garrido, C. (1995). Distribution of niobium, tantalum, and other highly incompatible trace elements in the lithospheric mantle: The spinel paradox. *Geochimica et Cosmochimica Acta* **60**, 545–550.

Bourdon, B., Eissen, J., Monzier, M., Robin, C., Martin, H., Cotten, J. & Hall, M. (2002). Adakite-like lavas from Antisana Volcano (Ecuador): evidence for slab melt metasomatism beneath the Andean Northern Volcanic Zone. *Journal of Petrology* **43**, 199–217.

Brenan, J., Shaw, H., Phinney, D. & Ryerson, F. (1994). Rutile–aqueous fluid partitioning of Nb, Ta, Hf, Zr, U and Th: implications for high field strength element depletions in island-arc basalts. *Earth and Planetary Science Letters* **128**, 327–339.

Brenan, J., Shaw, H. & Ryerson, F. (1995*a*). Experimental evidence for the origin of lead enrichments in convergent-margin magmas. *Nature* **378**, 54–56.

Brenan, J., Shaw, H., Ryerson, F. & Phinney, D. (1995*b*). Experimental determination of trace-element partitioning between pargasite and a synthetic hydrous andesitic melt. *Earth and Planetary Science Letters* **135**, 1–11.

Brenan, J., Shaw, H., Ryerson, F. & Phinney, D. (1995*c*). Mineral–aqueous fluid partitioning of trace elements at 900°C and 2·0 GPa: constraints on the trace element chemistry of mantle and deep crustal fluids. *Geochimica et Cosmochimica Acta* **59**, 3331–3350.

Capra, L., Macías, J. & Garduño, V. (1997). The Zitácuaro Volcanic Complex, Michoacán, México: magmatic and eruptive history of a resurgent caldera. *Geofísica Internacional* **36**, 161–179.

Carmichael, I. (2002). The andesite aqueduct: perspectives on the evolution of intermediate magmatism in west–central (105°–99°W) Mexico. *Contributions to Mineralogy and Petrology* **143**, 641–663.

Castillo, P., Janney, P. & Solidum, R. (1999). Petrology and geochemistry of Camiguin Island, southern Philippines: insights to the source of adakites and other lavas in a complex arc setting. *Contributions to Mineralogy and Petrology* **134**, 33–51.

Chesley, J., Ruiz, J., Righter, K., Ferrari, L. & Gómez-Tuena, A. (2002). Source contamination versus assimilation: an example from the Trans-Mexican Volcanic Arc. *Earth and Planetary Science Letters* **195**, 211–221.

Class, C., Miller, D. M., Goldstein, S. L. & Langmuir, C. H. (2000). Distinguishing melt and fluid subduction components in Umnak Volcanics, Aleutian Arc. *Geochemistry, Geophysics, Geosystems* **1**, doi:10.1029/1999GC000010.

Conrey, R., Hooper, P., Larson, P., Chesley, J. & Ruiz, J. (2001). Trace element and isotopic evidence for two types of crustal melting beneath a High Cascade volcanic center, Mt. Jefferson, Oregon. *Contributions to Mineralogy and Petrology* **141**, 710–732.

Defant, M. & Drummond, M. (1990). Derivation of some modern arc magmas by melting of young subducted lithosphere. *Nature* **347**, 662–665.

DePaolo, D. (1981). Trace element and isotopic effects of combined wallrock assimilation and fractional crystallization. *Earth and Planetary Science Letters* **53**, 189–202.

Donnelly, K. (2002). The genesis of E-MORB: extensions and limitations of the hot spot model. Ph.D. thesis, Columbia University, New York.

Drummond, M. & Defant, M. (1990). A model for trondhjemite–tonalite–dacite genesis and crustal growth via slab melting: Archean to modern comparisons. *Journal of Geophysical Research* **95**, 21505–21521.

Elburg, M., Van Bergen, M., Hoogewerff, J., Foden, J., Vroon, P., Zulkarnain, I. & Nasution, A. (2002). Geochemical trends across an arc–continent collision zone: magma sources and slab-wedge transfer processes below the Pantar Strait volcanoes, Indonesia. *Geochimica et Cosmochimica Acta* **66**, 2771–2789.

Elliott, T., Plank, T., Zindler, A., White, W. & Bourdon, B. (1997). Element transport from slab to volcanic front at the Mariana arc. *Journal of Geophysical Research* **102**, 14991–15019.

Ferrari, L. (2004). Slab detachment control on mafic volcanic pulse and mantle heterogeneity in central Mexico. *Geology* **32**, 77–80.

Foley, S., Barth, M. & Jenner, G. (2000). Rutile/melt partition coefficients for trace elements and an assessment of the influence of rutile on the trace element characteristics of subduction zone magmas. *Geochimica et Cosmochimica Acta* **64**, 933–938.

Foley, S., Tiepolo, M. & Vannucci, R. (2002). Growth of the early continental crust controlled by melting of amphibolite in subduction zones. *Nature* **417**, 837–840.

Garrison, J. & Davidson, J. (2003). Dubious case for slab melting in the Northern volcanic zone of the Andes. *Geology* **31**, 565–568.

Gill, J. (1981). *Orogenic Andesites and Plate Tectonics*. Berlin: Springer.

Gómez-Tuena, A., LaGatta, A., Langmuir, C., Goldstein, S., Ortega-Gutiérrez, F. & Carrasco-Núñez, G. (2003). Temporal control of subduction magmatism in the Eastern Trans-Mexican Volcanic Belt: mantle sources, slab contributions and crustal contamination. *Geochemistry, Geophysics, Geosystems* **4**, doi:10.1029/2003GC000524.

Green, T. & Pearson, N. (1987). An experimental study of Nb and Ta partitioning between Ti-rich minerals and silicate liquids at high pressure and temperature. *Geochimica et Cosmochimica Acta* **51**, 55–62.

Green, T. H. (1995). Significance of Nb/Ta as an indicator of geochemical processes in the crust mantle system. *Chemical Geology* **120**, 347–359.

Green, T. H. & Pearson, N. (1986). Ti-rich accessory phase saturation in hydrous mafic–felsic compositions at high *P, T*. *Chemical Geology* **54**, 185–201.

Hart, S. & Dunn, T. (1993). Experimental cpx/melt partitioning of 24 trace elements. *Contributions to Mineralogy and Petrology* **113**, 1–8.

Hildreth, W. & Moorbath, S. (1988). Crustal contributions to arc magmatism in the Andes of central Chile. *Contributions to Mineralogy and Petrology* **98**, 455–489.

Hirose, K. (1997). Melting experiments on lherzolite KLB-1 under hydrous conditions and generation of high-magnesian andesites. *Geology* **25**, 42–44.

Hochstaedter, A., Gill, J., Peters, R., Broughton, P. & Holden, P. (2001). Across-arc geochemical trends in the Izu–Bonin arc: contributions from the subducting slab. *Geochemistry, Geophysics, Geosystems* **2**, doi:10.1029/2000GC000105.

Hou, Z., Gao, Y., Qu, X., Rui, Z. & Mo, X. (2004). Origin of adakitic intrusives generated during mid-Miocene east–west extension in southern Tibet. *Earth and Planetary Science Letters* **220**, 139–155.

Ionov, D., Grégoire, M. & Prikhod'ko, V. (1999). Feldspar–Ti-oxide metasomatism in off-cratonic continental and oceanic upper mantle. *Earth and Planetary Science Letters* **165**, 37–44.

Irvine, T. & Baragar, W. (1971). A guide to the chemical classification of the common volcanic rocks. *Canadian Journal of Earth Sciences* **8**, 523–548.

Johnson, K. (1994). Experimental cpx/and garnet/melt partitioning of REE and other trace elements at high pressures; petrogenetic implications. *Mineralogical Magazine* **58A**, 454–455.

Johnson, M. & Plank, T. (1999). Dehydration and melting experiments constrain the fate of subducted sediments. *Geochemistry, Geophysics, Geosystems* **1**, doi:10.1029/1999GC000014.

Kalfoun, F., Ionov, D. & Merlet, C. (2002). HFSE residence and Nb/Ta ratios in metasomatised, rutile-bearing mantle peridotites. *Earth and Planetary Science Letters* **199**, 49–65.

Kay, R. (1978). Aleutian magnesian andesites: melts from subduction Pacific Oceanic crust. *Journal of Volcanology and Geothermal Research* **4**, 117–132.

Kelemen, P., Hanghøj, K. & Greene, A. (2003). One view of the geochemistry of subduction-related magmatic arcs, with emphasis on primitive andesite and lower crust. In: Rudnick, R. (ed.) *Treatise on Geochemistry.* New York: Elsevier, pp. 593–659.

Kelemen, P., Yogodzinski, G. & Scholl, D. (2004). Along-strike variation in lavas of the Aleutian Island Arc: implications for the genesis of high Mg-number andesite and the continental crust. In: Eiler, J. (ed.) *Inside the Subduction Factory. Geophysical Monograph, American Geophysical Union* **138**, 223–276.

Kelemen, P. B. (1998). Silica enrichment in the continental upper mantle via melt/rock reaction. *Earth and Planetary Science Letters* **164**, 387–406.

Kelemen, P. B., Shimizu, N. & Dunn, T. (1993). Relative depletion of niobium in some arc magmas and the continental crust: partitioning of K, Nb, La and Ce during melt/rock interaction in the upper mantle. *Earth and Planetary Science Letters* **120**, 111–134.

Keppler, H. (1996). Constraints from partitioning experiments on the composition of subduction-zone fluids. *Nature* **380**, 237–240.

Kessel, R., Schmidt, M., Ulmer, P. & Pettke, T. (2005). Trace element signature of subduction-zone fluids, melts and supercritical liquids at 120–180 km depth. *Nature* **437**, 724–727.

LaGatta, A. (2003). Arc magma genesis in the eastern Mexican volcanic belt. Ph.D. thesis, Columbia University, New York.

Lassiter, J. & Luhr, J. (2001). Osmium abundance and isotope variations in mafic Mexican volcanic rocks: evidence for crustal contamination and constraints on the geochemical behavior of osmium during partial melting and fractional crystallization. *Geochemistry, Geophysics, Geosystems* **2**, doi:10.1029/2000GC000116.

Lehnert, K., Su, Y., Langmuir, C., Sarbas, B. & Nohl, U. (2000). A global geochemical database structure for rocks. *Geochemistry, Geophysics, Geosystems* **1**, doi:10.1029/1999GC000026.

Le Maitre, R. (1989). *A Classification of Igneous Rocks and Glossary of Terms.* Oxford: Blackwell.

Lozano, R., Verma, S., Giron, P., Velasco, F., Morán-Zenteno, D., Viera, F. & Chávez, G. (1995). Calibración preliminar de fluorescencia de rayos X para análisis cuantitativo de elementos mayores en rocas ígneas. *Actas INAGEQ* **1**, 203–208.

Luhr, J. (2000). The geology and petrology of Volcan San Juan Nayarit, Mexico and the compositionally zoned Tepic Pumice. *Journal of Volcanology and Geothermal Research* **95**, 109–156.

Luhr, J. & Carmichael, I. (1985*a*). Contemporaneous eruptions of calc-alkaline and alkaline magmas along the volcanic front of the Mexican Volcanic Belt. *Geofísica Internacional* **24**, 203–216.

Luhr, J. & Carmichael, I. (1985*b*). Jorullo Volcano, Michoacán, Mexico (1759–1774): the earliest stages of fractionation in calc-alkaline magmas. *Contributions to Mineralogy and Petrology* **90**, 142–161.

Luhr, J., Allan, J., Carmichael, I., Nelson, S. & Hasenaka, T. (1989). Primitive calc-alkaline and alkaline rock types from the western Mexican volcanic belt. *Journal of Geophysical Research* **94**, 4515–4530.

MacPherson, C., Dreher, S. & Thirlwall, M. F. (2006). Adakites without slab melting: high pressure differentiation of island arc magma, Mindanao, the Philippines. *Earth and Planetary Science Letters* **243**, 581–593.

Manea, M., Manea, V. & Kostoglodov, V. (2003). Sediment fill in the Middle America Trench inferred from gravity anomalies. *Geofísica Internacional* **42**, 603–612.

Manea, V., Manea, M., Kostoglodov, V., Currie, C. & Sewell, G. (2004). Thermal structure, coupling and metamorphism in the Mexican subduction zone beneath Guerrero. *Geophysical Journal International* **158**, 775–784.

Manea, V., Manea, M., Kostoglodov, V. & Sewell, G. (2005). Thermo-mechanical model of the mantle wedge in Central Mexican subduction zone and a blob tracing approach for the magma transport. *Physics of the Earth and Planetary Interiors* **149**, 165–186.

Márquez, A., Oyarzún, R., Doblas, M. & Verma, S. (1999). Alkalic (oceanic-island basalt type) and calc-alkalic volcanism in the Mexican volcanic belt: a case for plume-related magmatism and propagating rifting at an active margin? *Geology* **27**, 51–54.

Martin, H. (1999). The adakitic magmas: modern analogues of Archaean granitoids. *Lithos* **46**, 411–429.

Martínez-Serrano, R., Schaaf, P., Solís-Pichardo, G., Hernández-Bernal, M., Hernández-Treviño, T., Morales-Contreras, J. & Macías, J. (2004). Sr, Nd and Pb isotope and geochemical data from the Quaternary Nevado de Toluca volcano, a source of recent adakitic magmatism, and the Tenango Volcanic Field, Mexico. *Journal of Volcanology and Geothermal Research* **138**, 77–110.

McCulloch, M. & Gamble, J. (1991). Geochemical and geodynamical constraints on subduction zone magmatism. *Earth and Planetary Science Letters* **102**, 358–374.

Moore, G. & Shipley, T. (1988). Mechanisms of sediment accretion in the Middle America Trench. *Journal of Geophysical Research* **93**, 8911–8927.

Moore, J., Watkins, J., Bachman, S., Beghtel, F., Butt, A., Didyk, B., Foss, G., Leggett, J., Lundberg, N., McMillan, N., Niitsuma, N., Shephard, L., Stephen, J., Shipley, T. & Strander, H. (1982). Facies belts of the Middle America Trench and forearc region, southern Mexico: results from Leg 66 DSDP. In: Legget, J. K. (ed.) *Trench–Forearc Geology: Sedimentation and Tectonics on Modern and Ancient Active Plate Margins. Geological Society, London, Special Publications* **10**, 77–94.

Müntener, O., Kelemen, P. & Grove, T. (2001). The role of H_2O during crystallization of primitive arc magmas under uppermost mantle conditions and genesis of igneous pyroxenites: an experimental study. *Contributions to Mineralogy and Petrology* **141**, 643–658.

Pardo, M. & Suárez, G. (1995). Shape of the subducted Rivera and Cocos plate in southern Mexico: seismic and tectonic implications. *Journal of Geophysical Research* **100**, 12357–12373.

Pearce, J., Stern, C., Bloomer, S. & Fryer, P. (2005). Geochemical mapping of the Mariana arc–basin system: implications for the nature and distribution of subduction components. *Geochemistry, Geophysics, Geosystems* **6**, doi:10.1029/2004GC000895.

Petrone, C., Francalanci, L., Carlson, R., Ferrari, L. & Conticelli, S. (2003). Unusual coexistence of subduction-related and intraplate-type magmatism: Sr, Nd and Pb isotope and trace element data from the magmatism of the San Pedro–Ceboruco graben (Nayarit, Mexico). *Chemical Geology* **193**, 1–24.

Pier, J., Podosek, F., Luhr, J., Brannon, J. & Aranda-Gómez, J. (1989). Spinel-lherzolite-bearing Quaternary volcanic centers in

San Luis Potosi, Mexico 2. Sr and Nd isotopic systematics. *Journal of Geophysical Research* **94**, 7941–7951.

Plank, T. & Langmuir, C. (1998). The chemical composition of subducting sediment and its consequences for the crust and mantle. *Chemical Geology* **145**, 325–394.

Poli, S. & Schmidt, M. (2002). Petrology of subducted slabs. *Annual Review of Earth and Planetary Sciences* **30**, 207–235.

Prouteau, G., Scaillet, B., Pichavant, M. & Maury, R. (1999). Fluid-present melting of oceanic crust in subduction zones. *Geology* **27**, 1111–1114.

Prouteau, G., Scaillet, B., Pichavant, M. & Maury, R. (2001). Evidence for mantle metasomatism by hydrous silicic melts derived from subducted oceanic crust. *Nature* **410**, 197–200.

Rapp, R. (1995). The amphibole-out phase boundary in partially melted metabasalt, and its control over melt fraction and composition, and source permeability. *Journal of Geophysical Research* **100**, 15601–15610.

Rapp, R. & Watson, E. (1995). Dehydration melting of metabasalt at 8–32 kbar: implications for continental growth and crust–mantle recycling. *Journal of Petrology* **36**, 891–931.

Rapp, R., Shimizu, N., Norman, M. & Applegate, G. (1999). Reaction between slab-derived melts and peridotite in the mantle wedge: experimental constraints at 3·8 GPa. *Chemical Geology* **160**, 335–256.

Rapp, R., Shimizu, N. & Norman, M. (2003). Growth of early continental crust by partial melting of eclogite. *Nature* **425**, 605–609.

Rollinson, H. (1993). *Using Geochemical Data*. Harlow: Longman.

Ruiz, J., Patchett, P. & Arculus, R. (1988*a*). Nd–Sr isotope constraints of lower crustal xenoliths—evidence for the origin of mid-Tertiary felsic volcanics in Mexico. *Contributions to Mineralogy and Petrology* **99**, 36–43.

Ruiz, J., Patchett, P. & Ortega-Gutiérrez, F. (1988*b*). Proterozoic and Phanerozoic basement terranes of Mexico from Nd isotopic studies. *Geological Society of America Bulletin* **100**, 274–281.

Ryerson, F. & Watson, E. (1987). Rutile saturation in magmas—implications for Ti–Nb–Ta depletion in island-arc basalts. *Earth and Planetary Science Letters* **86**, 225–239.

Salters, V. & Longhi, J. (1999). Trace element partitioning during the initial stages of melting beneath mid-ocean ridges. *Earth and Planetary Science Letters* **166**, 15–30.

Schaaf, P., Heinrich, W. & Besch, T. (1994). Composition and Sm–Nd isotopic data of the lower crust beneath San Luis Potosí, central Mexico: evidence from a granulite-facies xenolith suite. *Chemical Geology* **118**, 63–84.

Schaaf, P., Stimac, J., Siebe, C. & Macías, J. (2005). Geochemical evidence for mantle origin and crustal processes in volcanic rocks from Popocatépetl and surrounding monogenetic volcanoes, central Mexico. *Journal of Petrology* **46**, 1243–1282.

Schiano, P., Clocchiatti, R., Shimizu, N., Weis, D. & Mattielli, N. (1994). Cogenetic silica-rich and carbonate-rich melts trapped in mantle minerals in Kerguelen ultramafic xenoliths: implications for metasomatism in the oceanic upper mantle. *Earth and Planetary Science Letters* **123**, 167–178.

Schiano, P., Clocchiatti, R., Shimizu, N., Maury, R., Jochum, K. & Hoffman, A. (1995). Hydrous, silica-rich melts in the sub-arc mantle and their relationship with erupted arc lavas. *Nature* **377**, 595–600.

Schmidt, M. & Poli, S. (1998). Experimentally based water budgets for dehydrating slabs and consequences for arc magma generation. *Earth and Planetary Science Letters* **163**, 361–379.

Schmidt, M., Dardon, A., Chazot, G. & Vannucci, R. (2004). The dependence of Nb and Ta rutile–melt partitioning on melt composition and Nb/Ta fractionation during subduction processes. *Earth and Planetary Science Letters* **226**, 415–432.

Schneider, M. & Eggler, D. (1986). Fluids in equilibrium with peridotite minerals: implications for mantle metasomatism. *Geochimica et Cosmochimica Acta* **50**, 711–724.

Sen, C. & Dunn, T. (1994). Dehydration melting of a basaltic composition amphibolite at 1·5 and 2·0 GPa: implications for the origin of adakites. *Contributions to Mineralogy and Petrology* **117**, 394–409.

Siebe, C., Rodríguez-Lara, V., Schaaf, P. & Abrams, M. (2004). Geochemistry, Sr–Nd isotope composition, and tectonic setting of Holocene Pelado, Guespalapa and Chichinautzin scoria cones, south of Mexico City. *Journal of Volcanology and Geothermal Research* **2712**, 1–30.

Smith, D. & Leeman, W. (1996). The origin of Mount St. Helens andesites. *Journal of Volcanology and Geothermal Research* **55**, 271–303.

Stadler, R., Foley, S., Brey, G. & Horn, I. (1998). Mineral–aqueous fluid partitioning of trace elements at 900–1200°C and 3·0–5·7 GPa: new experimental data for garnet, clinopyroxene, and rutile, and implications for mantle metasomatism. *Geochimica et Cosmochimica Acta* **62**, 1781–1801.

Stern, C. & Kilian, R. (1996). Role of the subducted slab, mantle wedge and continental crust in the generation of adakites from the Andean Austral volcanic vone. *Contributions to Mineralogy and Petrology* **123**, 263–281.

Stolz, A., Jochum, K., Spettel, B. & Hofmann, A. W. (1996). Fluid- and melt-related enrichment in the subarc mantle: evidence from Nb/Ta variation in arc basalts. *Geology* **24**, 587–590.

Straub, S. & Martin-Del Pozzo, A. (2001). The significance of phenocryst diversity in tephra from recent eruptions at Popocatépetl Stratovolcano (central Mexico). *Contributions to Mineralogy and Petrology* **140**, 487–510.

Straub, S., Layne, G., Schmidt, A. & Langmuir, C. (2004). Volcanic glasses at the Izu arc volcanic front: new perspectives on fluid and sediment melt recycling in subduction zones. *Geochemistry, Geophysics, Geosystems* **5**, doi:10.1029/2002GC000408.

Sun, S. & McDonough, W. (1989). Chemical and isotopic systematics of oceanic basalts: implications for mantle compositions and processes. In: Saunders, A. D. & Norry, M. J. (eds) *Magmatism in the Ocean Basins. Geological Society, London, Special Publications* **42**, 313–345.

Tatsumi, Y. (2001). Geochemical modeling of partial melting of subducting sediments and subsequent melt–mantle interaction: generation of high-Mg andesites in the Setouchi volcanic belt, southwest Japan. *Geology* **29**, 323–326.

Tatsumi, Y. & Hanyu, T. (2003). Geochemical modeling of dehydration and partial melting of subducting lithosphere: toward a comprehensive understanding of high-Mg andesite formation in the Setouchi volcanic belt, SW Japan. *Geochemistry, Geophysics, Geosystems* **4**, doi:10.1029/2003GC000530.

Tiepolo, M., Vannucci, R., Oberti, R., Foley, S., Bottazzi, P. & Zanetti, A. (2000). Nb and Ta incorporation and fractionation in titanian pargasite and kaersutite: crystal-chemical constraints and implications for natural systems. *Earth and Planetary Science Letters* **176**, 185–201.

Todt, W., Cliff, R., Hanser, A. & Hofmann, A. W. (1996). Evaluation of a ^{202}Pb–^{205}Pb double spike for high-precision lead isotope analysis. In: Basu, A. & Hart, S. (eds) *Earth Processes: Reading the Isotopic Code. Geophysical Monograph, American Geophysical Union* **95**, 429–437.

van Westrenen, W., Blundy, J. & Wood, B. (2001). High field strength element/rare earth fractionation during partial melting in the presence of garnet: implications for identifications of mantle heterogeneities. *Geochemistry, Geophysics, Geosystems* **2**, doi:10.1029/2000GC000133.

Verma, S. (1999). Geochemistry of evolved magmas and their relationship to subduction-unrelated mafic volcanism at the volcanic front of the central Mexican Volcanic Belt. *Journal of Volcanology and Geothermal Research* **93**, 151–171.

Verma, S. (2000*a*). Geochemical evidence for a lithospheric source for magmas from Los Humeros caldera, Puebla, Mexico. *Chemical Geology* **164**, 35–60.

Verma, S. (2000*b*). Geochemistry of the subducting Cocos plate and the origin of subduction-unrelated mafic volcanism at the front of the central Mexican Volcanic Belt. In: Delgado-Granados, H., Aguirre-Díaz, G. & Stock, J. (eds) *Cenozoic Tectonics and Volcanism of Mexico. Geological Society of America, Special Papers* **334**, 1–28.

Verma, S. (2002). Absence of Cocos plate subduction-related basic volcanism in southern Mexico: a unique case on Earth? *Geology* **30**, 1095–1098.

Wallace, P. & Carmichael, I. (1999). Quaternary volcanism near the Valley of Mexico: implications for subduction zone magmatism and the effects of crustal thickness variations on primitive magma compositions. *Contributions to Mineralogy and Petrology* **135**, 291–314.

Wang, Q., McDermott, F., Xu, J., Bellon, H. & Zhu, Y. (2005). Cenozoic K-rich adakitic volcanic rocks in the Hohxil area, northern Tibet: lower-crustal melting in an intracontinental setting. *Geology* **33**, 465–468.